Journal of Geophysical Research: Earth Surface

RESEARCH ARTICLE
10.1002/2017JF004468

Key Points:
- Sea-swell waves drive most suspended sediment variability but infragravity waves and/or mean currents contribute to subtidal variability
- Reduced bed stresses within large bottom roughness are still greater than those on a sandy bed within the lagoon without roughness
- Limited sediment availability on a reef flat reduces suspended sediment concentrations compared to within reef lagoon and channels

Spatial Variability of Sediment Transport Processes Over Intratidal and Subtidal Timescales Within a Fringing Coral Reef System

Andrew W. M. Pomeroy[1,2,3], Ryan J. Lowe[1,2,3,4], Marco Ghisalberti[5,6], Gundula Winter[1,2,3], Curt Storlazzi[7], and Michael Cuttler[2,3,4]

[1]Oceans Graduate School, The University of Western Australia, Crawley, Western Australia, Australia, [2]The UWA Oceans Institute, The University of Western Australia, Crawley, Western Australia, Australia, [3]ARC Centre of Excellence for Coral Reef Studies, The University of Western Australia, Crawley, Western Australia, Australia, [4]School of Earth Sciences, The University of Western Australia, Crawley, Western Australia, Australia, [5]Department of Infrastructure Engineering, The University of Melbourne, Parkville, Victoria, Australia, [6]School of Civil, Environmental and Mining Engineering, The University of Western Australia, Crawley, Western Australia, Australia, [7]Pacific Coastal and Marine Science Center, U.S. Geological Survey, Santa Cruz, CA, USA

Abstract Sediment produced on fringing coral reefs that is transported along the bed or in suspension affects ecological reef communities as well as the morphological development of the reef, lagoon, and adjacent shoreline. This study quantified the physical process contribution and relative importance of sea-swell waves, infragravity waves, and mean currents to the spatial and temporal variability of sediment in suspension. Estimates of bed shear stresses demonstrate that sea-swell waves are the key driver of the suspended sediment concentration (SSC) variability spatially (reef flat, lagoon, and channels) but cannot fully describe the SSC variability alone. The comparatively small but statistically significant contribution to the bed shear stress by infragravity waves and currents, along with the spatial availability of sediment of a suitable size and volume, is also important. Although intratidal variability in SSC occurs in the different reef zones, the majority of the variability occurs over longer slowly varying (subtidal) timescales, which is related to the arrival of large swell waves at a reef location. The predominant flow pathway, which can transport suspended sediment, consists of cross-reef flow across the reef flat that diverges in the lagoon and returns offshore through channels. This pathway is primarily due to subtidal variations in wave-driven flows but can also be driven alongshore by wind stresses when the incident waves are small. Higher frequency (intratidal) current variability also occurs due to both tidal flows and variations in the water depth that influence wave transmission across the reef and wave-driven currents.

Correspondence to:
A. W. M. Pomeroy,
andrewpomeroy@gmail.com

Citation:
Pomeroy, A. W. M., Lowe, R. J., Ghisalberti, M., Winter, G., Storlazzi, C., & Cuttler, M. (2018). Spatial variability of sediment transport processes over intratidal and subtidal timescales within a fringing coral reef system. *Journal of Geophysical Research: Earth Surface*, *123*, 1013–1034. https://doi.org/10.1002/2017JF004468

Received 21 AUG 2017
Accepted 4 MAR 2018
Accepted article online 23 MAR 2018
Published online 17 MAY 2018

1. Introduction

Sediment is produced in coral reefs by mechanical and biological erosion of the reef framework as part of a constructive and destructive cycle (e.g., Chave et al., 1972; Scoffin, 1992; Stearn et al., 1977). The transport of this sediment influences the environmental conditions that benthic reef organisms experience, ranging from low turbidity environments (e.g., Acevedo et al., 1989; Buddemeier & Hopley, 1988; Rogers, 1990) to highly turbid environments (e.g., Anthony, 2000; Larcombe et al., 2001; Roy & Smith, 1971; Tudhope & Scoffin, 1994). This sediment is also redistributed throughout the coral reef where it can be deposited on the reef surface (e.g., Harney & Fletcher, 2003; Storlazzi et al., 2009), be re-incorporated into the reef structure (e.g., Hubbard, 1986; Perry & Hepburn, 2008), infill lagoons (e.g., Kench, 1998b; Kennedy & Woodroffe, 2000), construct shoreline or reef island geomorphic features (e.g., Perry et al., 2011; Sanderson & Eliot, 1996; Woodroffe et al., 1999), or be exported from the reef system via channels or breaks in the reef (e.g., Hine et al., 1981; Hughes, 1999; Storlazzi et al., 2004).

Increased sediment transport caused by both natural and anthropogenic disturbances above typical (baseline) environmental conditions often affect the health of reef communities through light attenuation (e.g., Roth, 2014; Storlazzi et al., 2015) and sedimentation (e.g., Anthony, 2000), which when reaching critical exposure conditions, can eventually lead to mortality (e.g., Jokiel et al., 2014; Weber et al., 2012). The critical exposure concentration and period for different species have been found to vary over several orders of magnitude, ranging from hours to a number of weeks (see Erftemeijer et al., 2012, for a review). The loss of these

reef organisms, in turn, affects the sediment production. Although the impact of sediment on reef organisms has been the subject of considerable interest, the detailed physical mechanisms that govern sediment transport (and ultimately the development of geomorphic features) in reef environments are less well understood. This is due to the high degree of spatial and temporal variability in the processes that can influence reef ecosystems across a range of scales.

Sediment motion is initiated, in general, when bed shear stresses (τ) imposed by currents and waves on an unconsolidated bed of sediment exceed a critical threshold for the sediment. This critical threshold depends on the sediment density and grain size properties (Shields, 1936). If the seabed is bare (e.g., lacking large immobile roughness associated with reef communities), the shear stresses imposed at the sediment interface can be directly estimated from the overlying current and wave conditions (e.g., Nielsen, 1992). However, in the presence of large immobile roughness (often referred to as canopies), these stresses can be substantially reduced due to attenuation of the current and waves (e.g., Le Bouteiller & Venditti, 2015; Pomeroy et al., 2017; Stocking et al., 2016). Once sediment motion has been initiated, the sediment is initially transported as bedload, which may include the migration of bed forms such as ripples (e.g., Traykovski et al., 1999; Van Rijn, 1984a). When the vertical component of turbulent eddies generated near the bed are sufficiently large to overcome the particle fall velocity (w_s), the sediment can be lifted into suspension (e.g., Bagnold, 1966; Francis, 1973; Van Rijn, 1984b). If ripples are present, organized vortex shedding can also suspend sediment from the bed (e.g., O'Hara Murray et al., 2011; Thorne et al., 2003). Sediment in suspension is transported by mean currents until it can no longer be supported by the upward vertical component of the turbulent eddies or vortices; the suspended sediment then settles out of the water column and is deposited on the seabed. Thus, the magnitude, duration, and frequency of sediment transport events are directly related to the spatial and temporal variability of the hydrodynamic processes and the roughness properties of the seabed within a particular coastal region.

The physical characteristics of coral reef structures modify the spatial and temporal variability of hydrodynamic processes (i.e., waves and currents). The rapid transition in depth from relatively deep to shallow water on a fore reef slope transforms and dissipates sea-swell waves, predominantly by wave breaking but also due to bottom friction (e.g., Monismith, 2007). Sea-swell waves that do not break on the fore reef are limited by the water depth over the reef flat (e.g., Gourlay, 1994; Hardy & Young, 1996). As these waves propagate shoreward across the reef flat and into the lagoon, they can be further dissipated by the drag forces exerted by the large bottom roughness associated with reef communities (e.g., Lowe, Falter, et al., 2005), as well as through energy losses by nonlinear wave-wave interactions (e.g., Péquignet et al., 2014; Sheremet et al., 2011). In addition, as waves break in groups this can also lead to time-varying excursions of the short wave breakpoint and the generation of low frequency (infragravity) waves (Longuet-Higgins & Stewart, 1962; Symonds et al., 1982), which have been shown to be important in reef environments (e.g., Brander et al., 2004; Cheriton et al., 2016; Hardy & Young, 1996; Lugo-Fernández et al., 1998; Péquignet et al., 2009; Pomeroy et al., 2012; Roeber & Bricker, 2015). As a consequence, the wave spectrum across many reefs becomes bimodal and is usually characterized by depth-limited sea-swell waves with periods of 5–25 s and longer infragravity waves (periods of 25–250 s) that propagate across the reef.

Spatial gradients in radiation stresses that result from wave breaking on reefs (Longuet-Higgins & Stewart, 1964) are predominantly balanced by cross-shore pressure (wave setup) gradients and mean bottom stresses associated with cross-reef currents (e.g., Gourlay, 1996b, 1996a; Jago et al., 2007; Massel & Gourlay, 2000), but also in some areas of a reef (such as near channels) by advection (e.g., Taebi et al., 2012). For a one-dimensional reef with an unbounded lagoon, the relative magnitude of the wave-driven currents depends on radiation stress forcing that is modulated by the incident wave variability, changes in the reef water depth by tides, the bottom roughness properties, and the reef flat width (e.g., Gourlay & Colleter, 2005; Hearn, 1999; Symonds et al., 1995). When these cross-reef currents enter a coastally bounded lagoon (such as within a fringing reef), an alongshore pressure gradient is established where the sea level decreases toward gaps in the reef (e.g., Hench et al., 2008; Lowe et al., 2009). This pressure gradient drives currents through the lagoon and back to the surrounding ocean via the gaps in the reef (e.g., Coronado et al., 2007; Taebi et al., 2011).

Although the impact of a reef's morphology on wave transformations and the generation of currents and circulation has been the subject of considerable research, how these hydrodynamic processes drive the spatial and temporal variability in sediment transport remains unclear. Of the studies that have been

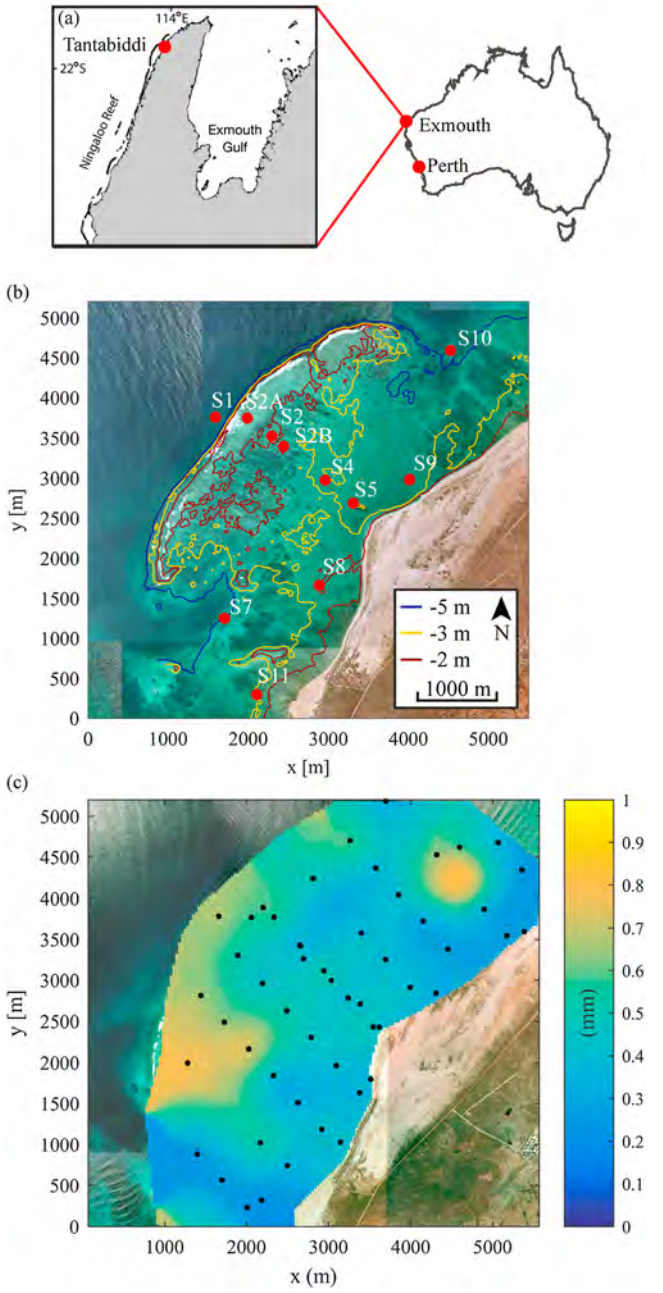

Figure 1. (a) The field study site at Tantabiddi within Ningaloo Reef in north-western Australia. (b) An aerial view of the site (origin: 21.89699°S, 113.96212°E) with the locations of the instruments employed in this study and key bathymetric contours. (c) Spatial distribution of the median (D_{50}) grain size. The black dots indicate sediment sampling sites.

undertaken, most have related suspended sediment concentration (SSC) variability to (short) sea-swell wave and current measurements (e.g., Kench, 1998a; Suhayda & Roberts, 1977; Vila-Concejo et al., 2014) or to shear stress estimates based on measurements usually obtained above the reef roughness (e.g., Harris et al., 2014; Ogston et al., 2004; Storlazzi et al., 2009), which may not reflect the stress experienced by sediment on the bed (Pomeroy et al., 2017). Furthermore, the role of infragravity waves on the transport of sediment in reefs remains poorly understood. Thus, there is a need to understand the physical process contribution and relative importance of sea-swell waves, infragravity waves, and mean currents within fringing reef systems to the spatial and temporal variability of sediment transport, as well as their implications for the quantity and transport pathway of sediment in suspension, which is the focus of this manuscript.

In section 2, we first describe a field experiment that focuses on a fringing reef in north-western Australia, including the instrument configurations and the data analysis methods. The results are then presented in section 3. In section 4, the implications of the spatial and temporal variability in both the hydrodynamics and SSCs for different reef zones are discussed. Finally, we present a synthesis of the study in the form of a conceptual model to characterize SSCs and suspended sediment fluxes within fringing coral reef-lagoon systems.

2. Methods

2.1. Site Description

The field study focused on a ~5-km section of reef near Tantabiddi (21°52′6.03″S, 113°58′58.26″E; Figure 1a) in Ningaloo Reef, Western Australia that (1) was exposed to temporally variable forcing conditions (waves, wind, and tides); (2) has a spatially-variable reef structure (reef flat with a clearly defined zonation and a sandy lagoon); and (3) exhibits large bottom roughness across the reef flat (formed by, e.g., coral reef communities, macroalgae, and relic limestone). This section of reef has a cross-shore orientation of ~130° (defined as clockwise from true north) and is bounded to the north and south by shore-normal channels that cut into the reef flat and reef crest. Due to the presence of the large salient at the shoreline in the lee of the reef, the location of the reef crest relative to the shoreline varies from 2.0 to 2.5 km. The reef flat is ~0.6–1.5 m below mean sea level at still water and is ~500 m in width. The lagoon is generally ~3 m deep with channels that are up to ~6 m deep and is characterized by a sandy bed.

The spatial distribution of bed sediment characteristics was obtained from ~500 g samples collected from the top 5 to 7 cm of the seabed across 73 sites spanning the range of subreef environments at the study area. The composition of these samples has previously been described in detail by Cuttler et al. (2015, 2017), and only a summary of the main results relevant to the present study are included here. Across the study area, the sediment was predominantly sand-sized, with silt-sized or smaller material (<0.063 mm) accounting for less than 3% at all sites except for the most shoreward sample in the south channel where mud and clay accounted for up to ~20%. There is a trend of decreasing median grain size from the reef crest (D_{50} of ~0.5 mm), shoreward through the lagoon (D_{50} of ~0.35 mm) to the beach (D_{50} of ~0.25 mm) as well as toward the north or south channel (Figure 3c). Although sediment on the southern side of the lagoon was slightly coarser than the northern side, the grain size variation was limited throughout the lagoon, with the majority of deposits classified as medium sands

Table 1
Constituent Assemblages for Bulk Sediment Samples From the Subreef Environments at Tantabiddi, Ningaloo Reef

Constituent	Reef crest (%)	Reef flat (%)	Lagoon (%)	Channel (%)	Beach (%)
Coral	37	38	36	27	33
Coralline algae	21	19	16	17	14
Mollusk	22	20	19	21	24
Foraminifera	8	7	7	5	6
Echinoderm	1	1	1	0	1
Framework	5	3	4	2	4
Quartz	5	5	16	28	18
Other	1	1	1	1	1

Note. From Cuttler et al. (2017).

(average D_{50} of ~0.35 mm). There was some variability in constituent assemblages across subreef environments. Coralline algae and reworked coral-derived grains exist in high proportions around the edges of the study area, adjacent to channels, while foraminifera and mollusk fragments are highest in the northwest corner of the study area. Quartz was only a dominant constituent (upward of 40%) near the shoreline (Table 1). In this study we focus on the SSCs measured on the reef flat at S2, in the lagoon at S5, and in the northern (S10) and southern (S7) channels. At these locations, the bed sediment distributions were similar with a D_{50} of ~0.3 mm.

The study area is located just north of a major tidal transition zone along Western Australia, which separates a diurnal and microtidal regime in southwestern Australia from the semidiurnal and macrotidal regime in the northwest. At this site, the tides are mixed, dominantly semidiurnal with a mean tidal range of 0.86 m and a maximum spring range of 1.5 m (Taebi et al., 2012). The monthly mean significant wave height incident to the site ranges from ~1 to 2 m with peak periods of ~11–15 s.

2.2. Field Study

A 3-week field experiment was conducted that consisted of two main components: (1) a detailed study of the hydrodynamics, SSC, and suspended sediment fluxes in the water column on the reef flat (Pomeroy et al., 2017), and (2) a broader-scale study of these same parameters throughout the reef and lagoon. The results presented in this manuscript focus on the latter component and are based on a large instrument array that quantified hydrodynamic processes and SSCs spatially throughout the study site. Detailed sampling information for each instrument is included in Table 2 and a summary follows.

The instrument array (Figure 1b) was deployed for a period of 19 days during the austral winter of 2013 (27 July to 14 August). Sea-swell wave conditions were measured on the fore reef at S1 with a 1-MHz Nortek AWAC directional wave gauge/current profiler. A cross-shore transect from near the reef crest to the tip of the shoreline salient measured the properties of waves that propagated toward the shoreline. In addition to the wave measurements, current profiles were measured by upward-facing Nortek acoustic Doppler profilers (ADP) toward the back of the reef flat (S2), as well as near the shoreline at the tip of the salient (S5). Two RDI Acoustic Doppler Current Profilers (ADCP) were also deployed in the southern and northern channels (S7 and S10). We note that due to the partial failure of the ADCP at S10, only wave measurements (from the ADCP pressure sensor) were obtained at that site. Close to the shoreline, the ADPs recorded current profiles and waves on either side of the salient (S8 and S9), and a wave gauge measured the wave conditions near the shoreline adjacent to the southern break in the reef (S11). The wind was measured at the Milyering weather station, approximately 20 km north of the site (Australian Institute of Marine Science, 2013).

Temporal variations in SSC were measured on the reef flat (S2) with Wetlabs FLNTU optical backscatter sensors (OBSs) and in the lagoon (S4), near the salient (S5), and in the channels (S7 and S10) with Aquatec 210-TY Loggers with Seapoint OBS Sensors. On the reef flat, direct in situ suction samples were obtained at hourly intervals during daylight hours via 5-mm diameter intakes, colocated with the OBSs, and oriented perpendicular to the dominant cross-reef flow direction (Bosman et al., 1987). The water samples were collected with peristaltic pumps, which pumped the samples to a scaffold platform nearby, and stored in 2-L bottles. The intake flow velocity was ~0.6 m/s, or two to three times greater than measured root mean squared velocities (see below); therefore, errors due to inefficiencies or bias in particle capture are expected to be small (Bosman et al., 1987). At the remaining OBS sites, in situ samples were obtained with 2.5-L Niskin bottles.

In addition to the fixed instrument array, nine to ten Lagrangian drifters, similar in design to those described by Schmidt et al. (2005), were deployed simultaneously to determine flow pathways and velocities over the reef. The drifters were deployed from a boat in predefined arrangements to isolate regions of different flow and were permitted to drift until they entered the channels or became stranded on the beach. The position of each drifter was recorded at 0.3 Hz by internal Garmin GPS devices (eTrex 10,

Table 2
Instrument Site Information and Sampling Configuration

Site	Depth (m)	Instrument	Sampling regime	Waves/pressure (m)[a]	Velocity profile[b]	SSC (m)[a]
S1 (fore reef)	~10.5	Nortek AWAC	1 Hz with 2,048 s burst every 3,600 s current profile every 5 min	—	1.04 m and 0.5 m cells	—
		RBR Virtuoso D	Continuous at 1 Hz	0.2	—	—
S2A (reef flat)	~1.3	RBR TWR-2050	4,096 samples at 2 Hz every 3,600	0.1	—	—
S2 (reef flat)	~1.5	Nortek ADP-HR	Continuous at 1 Hz	0.07	0.22 m with 25 mm cells	—
		Wetlabs FLNTU	0.29 Hz with 462 samples every 3,600 s	—	—	0.37, 0.64, 0.90
		Suction samples	Hourly during daylight	—	—	0.23, 0.27, 0.34, 0.51, 0.76, 1.02
S2B (reef flat)	~2.1	RBR Virtuoso D	Continuous at 1 Hz	0.05	—	
S4 (lagoon)	~2.7	RBR Virtuoso D	Continuous at 1 Hz	0.05	—	—
		Wetlabs FLNTU	Continuously every 15 s		—	0.28
S5 (salient)	~3.5	Nortek ADP	Continuous at 1 Hz	0.14	0.40 m with 10 cm cells	
		Aquatec 210-TY	Every 10 s continuously			0.55
S7 (south channel)	~5.4	RDI ADCP	Continuous at 1 Hz	0.33	1.07 m with 30 cm cells	
		Aquatec 210-TY	Every 10 s continuously		—	0.67
S8 (south salient)	~2.3	Nortek ADP	Current profile averaged over 180 s every 300 s 2,048 pressure samples at 2 Hz every 3,600 s	0.2	0.40 m with 10 cm cells	—
S9 (north salient)	~3.6	Nortek ADP	Current profile averaged over 180 s every 300 s 2,048 pressure samples at 2 Hz every 3,600 s	0.2	0.40 m with 10 cm cells	
S10 (north channel)	~7.4	RDI ADCP[c]	Continuous at 1 Hz	0.75	—	—
		Aquatec 210-TY	Continuously every 10 s		—	0.77
S11 (south channel)	~2.3	RBR T-Duo	2,048 samples at 1 Hz every 3,600 s	0.05	—	—

Note. Depth is relative to mean sea level.
[a]Measurement elevations are relative to the sea bed. [b]Elevation of first velocity profile measurement relative to the seabed. [c]Velocity measurements were not obtained due to an instrument fault.

position error of ±5 m recorded during the experiment). Ten drifter deployments (~2–4 hr each) were conducted under various wave, wind, and tidal conditions. A subset of these measurements is included in this study.

2.3. Hydrodynamic Data Analysis

Offshore wave conditions (wave height, period, and direction) were measured on the fore reef (S1) directly by the AWAC acoustic surface tracking, whereas wave conditions on the reef flat and in the lagoon were determined from conversion of the measured pressure time series using linear wave theory. Directional wave spectra were computed for sites on the fore reef, as well as at the sites where ADPs were deployed, using the Maximum Likelihood Method (Emery & Thomson, 2001). One-dimensional surface elevation spectra were derived from pressure time series at the other locations. From the spectra, the zeroth-moment (significant) wave heights for the shorter-period (5–25 s) sea-swell waves ($H_{m0,sw}$) and longer period (25–250 s) infragravity waves ($H_{m0,ig}$) were calculated, as well as both the peak period (T_P) and the weighted-mean sea-swell wave direction (θ) where colocated velocity measurements were available.

The raw ADP velocity measurements were initially filtered based on low signal correlations ($<$ 60%) before velocity spikes (e.g., caused by bubbles or debris in the sample volume) were removed using a kernel-based despiking algorithm (Goring & Nikora, 2002). Hourly currents were obtained for each ADP by reshaping the data into hourly bursts, for which the mean depth-averaged current speed (U) and direction were computed by averaging all samples in a burst in time and over all vertical bins. To quantify the hourly current variability along dominant flow directions, a principal component analysis was conducted.

To evaluate the variability in the currents and its relation to forcing variables over longer timescales, a low-pass PL66 filter (Beardsley et al., 1985) with a half-power period of 36 hr was applied to the depth-

averaged velocity measurements. We refer to the residual component (obtained by subtracting the subtidal signals from the original time series) as the intratidal variability. The spatial variability of the subtidal and intratidal circulation patterns was evaluated for the overlapping data using an empirical orthogonal function (EOF) analysis (Emery & Thomson, 2001). We note that the mean (time-averaged) currents were not removed from the depth-averaged current time series; therefore, this analysis was designed to maximize the total energy rather than the variance (Coronado et al., 2007).

The Lagrangian measurements of the flow pathways obtained from the drifters were isolated from the continuous data record, and small data gaps were linearly interpolated. The data were then low-pass filtered with a 60-s moving average.

2.4. Bed Shear Stresses

The total hydraulic resistance experienced by the flow (τ_{total}, equation (1)) can be partitioned into (1) a bed shear stress component (τ_{bed}) that acts directly on the sediment and thus is influenced by sediment properties; and (2) a form drag component (τ_{drag}) that is due to bed roughness that may be mobile (i.e., sand ripples; e.g., Van Rijn, 2007) or immobile (i.e., coral structures or aquatic vegetation; e.g., Le Bouteiller & Venditti, 2015):

$$\tau_{total} = \tau_{bed} + \tau_{drag} \tag{1}$$

In the presence of relatively small roughness, τ_{drag} is small and $\tau_{total} \approx \tau_{bed}$, which can be reasonably estimated from hydrodynamic measurements obtained above the bed (including higher in the water column), and is often expressed in terms of a bed shear velocity $\left(u* = \sqrt{\tau_{bed}/\rho_w}\right)$. However, when the bed roughness is large, τ_{drag} can be substantially greater than τ_{bed} and the shear stress/velocity estimated from hydrodynamic measurements obtained above the roughness is larger than that exerted on the sediment. For example, Pomeroy et al. (2017) demonstrated that the stresses imposed by large immobile roughness on the waves and currents above the roughness were unrelated to the suspension and transport of sediment on the reef flat at this site.

In addition to the influence of bed roughness on the calculation of u_*, nonlinear superposition of waves and currents (equation (2)) can enhance u_* such that the mean shear velocity (u_{*m}) is greater than the shear velocity associated with a pure current (u_{*c}) alone; and the maximum of this enhanced shear velocity (u_{*max}) is larger than the vector summation of u_{*c} and the wave shear velocity (u_{*w}; e.g., Soulsby & Clarke, 2005).

$$u_*^2 = u_{*c}^2 + u_{*w}^2 \tag{2}$$

On the reef flat at S2, the velocity measurements within the roughness layer were used to estimate the u_*, which eliminated the need to determine the reduction in velocity due to the large roughness on the reef flat (Pomeroy et al., 2017). In the sandy lagoon and channels that contained open sediment beds (no reef roughness), the velocity closest to the bed was used to estimate u_*. To account for the enhancement of the shear velocity in combined wave and current conditions, we adopted the approach by Madsen et al. (1988) and Madsen (1994) to calculate u_*, which extends the wave-current boundary layer theory of Grant and Madsen (1979) to spectral wave conditions. For each hourly burst of data, the mean current $(\overline{u})$ speed and direction were computed. We then used the Law of the Wall (equation (3)) to calculate u_{*c}:

$$u_{*c} = \frac{\overline{u}\kappa}{\log z - \log z_{0a}} \tag{3}$$

Here z is the height above the bed, κ is von Kármán's constant ($\kappa = 0.4$), and z_{0a} is an apparent roughness length that is enhanced by the wave-induced turbulence near the bed relative to a pure unidirectional current (e.g., Grant & Madsen, 1979).

To calculate u_{*w}, the mean current vector was removed from each velocity record, and the residual oscillatory (wave) velocity data were rotated into a coordinate system that maximized the velocity variance along the primary axis. In this coordinate system, the wave $(\widetilde{u})$ velocities were defined. For these spectral wave conditions, a representative near-bed horizontal orbital velocity $\widetilde{u}_r$ was calculated (e.g., Madsen, 1994; Madsen et al., 1988):

Table 3
Calibration Parameters Used for the Linear Conversion of the ADP and OBS Backscatter Data (B_k) to Suspended Sediment Concentration (SSC)

Site (instrument)	Calibration equation (mg/L)	R^2	n
S2 (ADP)	SSC = 0.052 B_k − 2.68	0.61	35
S5 (OBS)	SSC = 21.34 B_k − 2.22	0.99	12
S7 (OBS)	SSC = 4.78 B_k + 0.59	0.99	9
S10 (OBS)	SSC = 11.67 B_k − 3.21	0.99	12

Note. Calibration for the OBS instruments was conducted between the measured concentration and the instrument's recorded FTU. For all cases $p < 0.05$.

$$\widetilde{u}_r = \sqrt{\sum_{n=1}^{N} \widetilde{u}_n^2} \tag{4}$$

where $\widetilde{u}_n$ is the horizontal orbital velocity measurement of the nth frequency component. At S10 where near-bed wave-velocity data were not available due to the absence of high frequency velocity measurements, $\widetilde{u}_n$ was inferred from the pressure data using linear wave theory, that is,

$$\widetilde{u}_n = \frac{a_n \omega_n}{\sinh k_n h} \tag{5}$$

where ω_n is the radian frequency, a_n is the nth component of the wave amplitude as determined from the wave spectrum S by $a_n = \sqrt{2S_n df}$, k_n is the wave number, and h is the water depth. The representative wave radian frequency was defined as

$$\omega_r = \frac{\sum_{n=1}^{N} \omega_n \widetilde{u}_{b,n}^2}{\sum_{n=1}^{N} \widetilde{u}_{b,n}^2} \tag{6}$$

Finally, u_{*w} was obtained by relating $\widetilde{u}_r$ to a representative wave friction factor f_{wc}:

$$u_{*w} = \sqrt{\frac{1}{2} f_{wc} \widetilde{u}_r{}^2} \tag{7}$$

Many formulae for f_{wc} have been proposed, with most being a function of the bed roughness and the near-bed semi-orbital excursion. In this study, we used the explicit friction formula proposed by Madsen (1994), which assumes that monochromatic friction formulae for f_{wc} can be applied separately to each frequency component in a spectral wave field. Implicit in this assumption is that the representative hydraulic roughness length k_r is constant, which was found to be valid in laboratory experiments by Mathisen and Madsen (1999) and also reasonable in field observations over a coral reef flat by Lowe, Koseff, et al. (2005). To evaluate the spatial differences in the shear stresses imposed on sediment grains, we defined k_r using the Nikuradse roughness ($k_r = 2.5D_{50} \cong 30z_{0a}$). Differences in D_{50} only affected the calculated shear velocities by <10%.

To understand the relative importance of currents as well as sea-swell and infragravity waves to sediment transport, at each of the sites where SSC was calculated, we also calculated shear velocities separately for the contributions made by sea-swell (u_{*sw}) and infragravity (u_{*ig}) waves.

2.5. Suspended Sediment Concentrations

The water samples obtained near the OBS instruments were vacuum filtered onto preweighed membrane filters (Whatman ME27, 0.8 μm), dried (75°C for 24 hr), and weighed in order to calculate the SSC. To obtain a time series of SSC, the known values of SSC from the water samples were related to the measured backscatter via linear regression (Table 3). We note that for the ADP, this backscatter was also corrected for acoustic decay (e.g., Ha et al., 2011) prior to the regression analysis (see also Pomeroy et al., 2017).

The SSC variability at short timescales (<1 hr) was quantified by calculating the first and third concentration quartiles within the hourly data bursts. To evaluate the SSC variability over longer timescales, shorter bursts of data (15 min) were time-averaged to form a decimated time series that was then analyzed with the singular-spectrum analysis (SSA) technique (e.g., Schoellhamer, 2002; Vautard et al., 1992). This technique identifies a set of uncorrelated time-dependent variables that describe different fractions of the original signal variance. An advantage of this analysis technique in comparison to other techniques for SSC analysis is that it is nonparametric, which enables trends, as well as periodic or quasiperiodic components, to be identified that may also be amplitude modulated. In our analysis, we used a window period of M = 36 h for consistency with the low frequency cutoff for the hydrodynamics data.

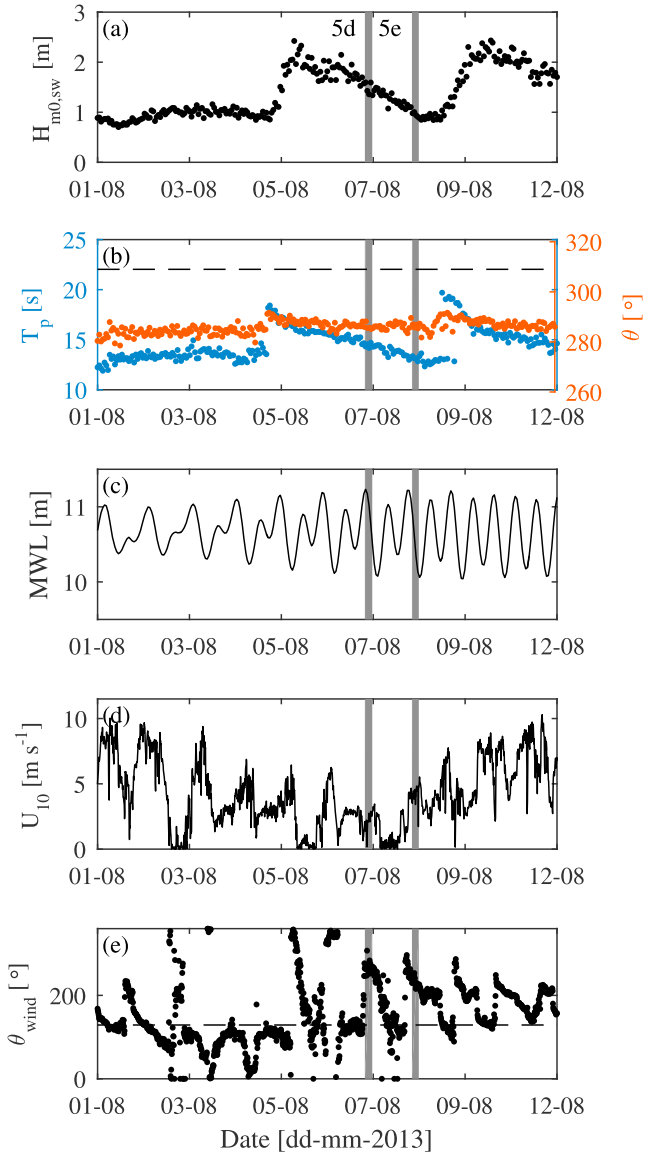

Figure 2. The offshore (a) swell wave height $H_{m0,sw}$; (b) peak wave period T_p and direction θ with cross-reef direction denoted by the horizontal dashed line; (c) water depth measured on the fore reef at S1; (d) the 10-min mean wind speed; and (e) the direction θ_{wind} measured in Nautical convention (0° and 360° indicates a southerly wind) at Milyering weather station. The horizontal dashed line in (e) indicates the offshore wind direction. The shaded bars refer to drifter deployments in Figure 5.

3. Results

3.1. Forcing Conditions

During the first part of the experiment (1–5 August), the offshore significant wave heights ($H_{m0,sw}$) measured on the fore reef at S1 were small and relatively constant (~0.7–1.2 m; Figure 2a). Two larger swell events (6–8 August and 9–12 August) occurred during the latter part of the experiment, with maximum wave heights reaching ~2.5 m during both events. T_p ranged from 12 s during the small wave conditions to as high as 19 s during the large swell events (Figure 2b). The $H_{m0,sw}$ measured on the fore reef at S1 originated from ~280° throughout the experiment (~30° from the cross-reef direction; Figure 2b), with very little variation in (±10°) during the swell events. The offshore water depth (Figure 2c) varied over the duration of the experiment, with the tidal range varying from ~0.6 m during neap tide to ~1.2 m during spring tide. The wind (Figures 2d and 2e) predominantly consisted of two states: (1) approximately offshore-directed winds and (2) approximately alongshore winds from the south. The offshore-directed winds occurred during the first part of the experiment (2–7 August) with speeds of 2–8 m/s. When the wind speeds decreased during this period, the direction of the wind changed and came from the north. Later in the experiment (7–12 August), distinct periods of alongshore winds from the south with speeds of 4–5 m/s occurred. When the southerly winds decreased during this period, the winds became predominantly offshore-directed. Overall, the winds tended to be stronger at the start and end of the experiment and were relatively weak during the first swell event (6–8 August); however, the wind increased with the arrival of the second swell event (9–12 August).

3.2. Waves

The height of the sea-swell waves ($H_{m0,sw}$) rapidly dissipated near the reef crest due to wave breaking, which occurred throughout the experiment and resulted in a much narrower range of wave conditions on the reef flat and in the lagoon (Figure 3a). The wave heights measured on the reef flat (sites S2, S2A, and S2B) were depth-limited and thus strongly correlated with the reef flat water depth (R^2 = 0.98) that varied over intratidal timescales (Figure 3c). When averaged over the entire experiment, the wave heights on the reef flat were ~25% of that measured on the fore reef at S1 but, depending on the water depth over the reef flat, could be ~5–40% of the S1 wave height. In contrast, the waves that entered through the channels (sites S7 and S10) were on average approximately twice as large as those measured on the reef flat. These waves were strongly correlated (R^2 = 0.87–0.92) with the offshore fore reef $H_{m0,sw}$, which was ~1.5–4 times larger than those in the channels. The waves measured in the channels were not strongly modulated by the tide but instead varied at longer (subtidal) timescales with variations in the offshore wave height (Figure 3c). Although the values of $H_{m0,sw}$ measured in the center of the lagoon (S4) were smaller than those on the reef flat and in the channels (i.e., ~5–25% of the $H_{m0,sw}$ measured at S1), closer to the shoreline (S5, S8, and S9), $H_{m0,sw}$ increased slightly due to refraction of the waves that propagated in from the channels (Figure 3c). This refraction resulted in some variability in wave direction at the tip of the salient at S5 (mean: 268°, range: 246–284°), but the waves were nearly perpendicular to the shoreline on either side of the salient (S8 and S9). The $H_{m0,sw}$ along the shoreline (S5, S8, S9, and S11) was similar throughout the study site (i.e., on average ~17% of S1 and varying by 7–36%). At sites in the lee of the reef (S5, S8, and S9), the $H_{m0,sw}$ values were correlated with the reef flat water depth (R^2 = 0.63–0.83), whereas the wave heights near the shoreline in line with the channel (S11) were strongly correlated (R^2 = 0.78) with the fore reef $H_{m0,sw}$.

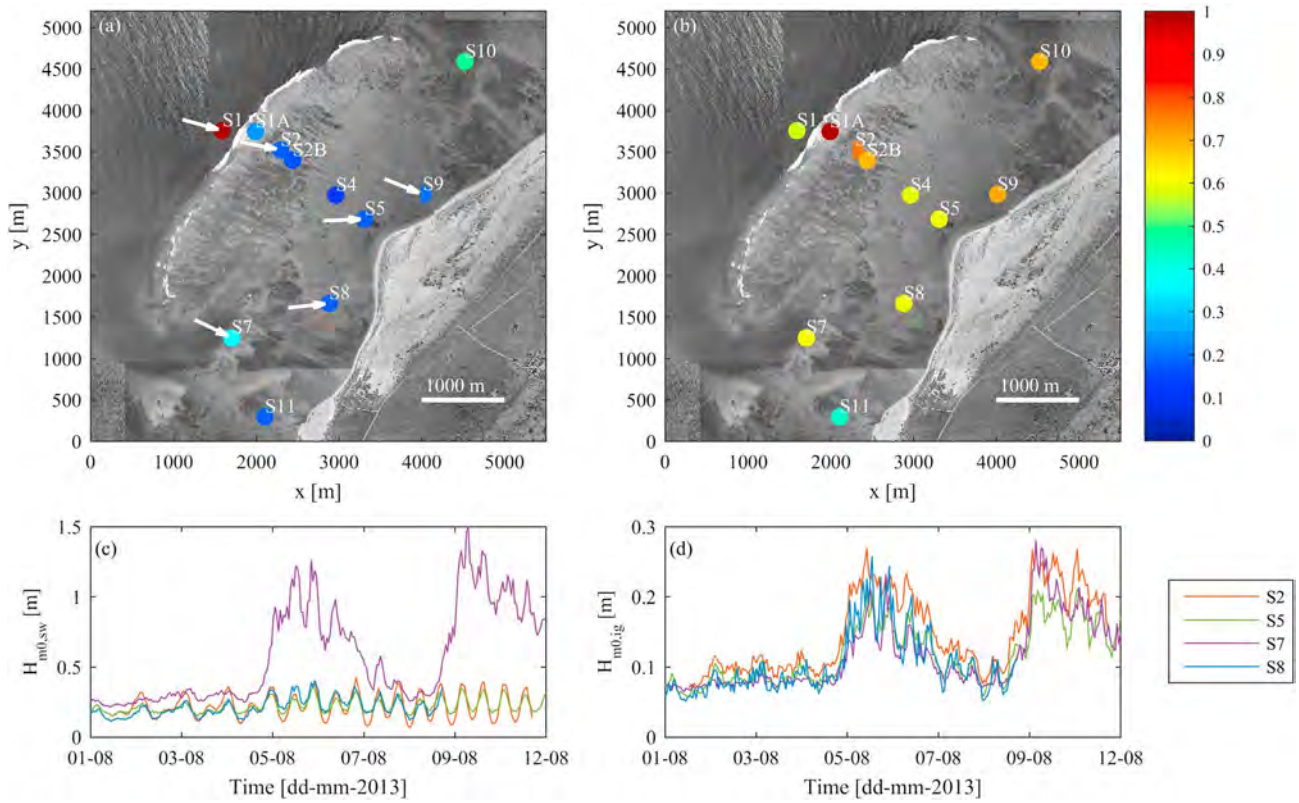

Figure 3. The mean over the entire experiment of (a) swell wave height $H_{m0,sw}$ normalized by $H_{m0,sw}$ at S1 with the mean wave direction indicated by the white arrows and (b) infragravity wave height $H_{m0,ig}$ at different measurement locations normalized by $H_{m0,ig}$ at S2A. The normalized wave height for (a) and (b) is indicated by the colorbar (no units). Time series of the (c) $H_{m0,sw}$ and (d) $H_{m0,ig}$ on the reef flat at S2 (red), in the lagoon at S5 (green), S8 (blue), and in the channel at S7 (purple).

The height of the infragravity waves ($H_{m0,ig}$) was largest on the reef flat near the reef crest (S2A; Figure 3b). $H_{m0,ig}$ decreased as the waves propagated through the lagoon (S4) toward the shoreline (S5, S8, and S9), where the waves were ~60–70% of the height measured at S2A when averaged over the experiment. These waves were not strongly modulated by the tidal elevation but instead were strongly correlated (R^2 = 0.92) with the offshore $H_{m0,sw}$ that varied over subtidal timescales (Figure 3d). As a consequence, the $H_{m0,sw}$ on the reef flat became larger than the $H_{m0,ig}$ during high tide but were similar or smaller in height at low tide as well as during the larger swell events. The $H_{m0,ig}$ values in the channels were also correlated (R^2 = 0.75–0.88) with the $H_{m0,sw}$ on the fore reef but were smaller than the $H_{m0,ig}$ measured on the reef flat (i.e., typically ~60–70% of the $H_{m0,ig}$ measured at S2A; Figure 3b).

3.3. Currents

The mean depth-averaged currents (U) on the reef flat (S2) were consistently directed cross-shore throughout the experiment (Figure 4) with a magnitude ranging from 0.03 to 0.12 m/s during the small swell periods to ~0.3 m/s during the large swell events. Near the salient (S5), the currents varied considerably in magnitude (~0.01–0.17 m/s) and direction ($\theta \approx 190 - 360^{\circ}$, indicated by the ellipses in Figure 4). Consequently, the mean current at this point could be directed to the north or south depending on the prevailing conditions. On either side of the salient at S8 and S9, the mean flows (~0.01–0.22 m/s) remained smaller than at S2 but were slightly larger than at S5 and were oriented mostly parallel to the adjacent shoreline (Figure 4). In the southern channel (S7), the mean currents were generally directed offshore ($\theta \approx 80 - 200^{\circ}$) through the channel but could be directed either offshore or onshore. To understand the processes responsible for the observed variability in magnitude and direction, the mean currents were decomposed into a subtidal and intratidal component.

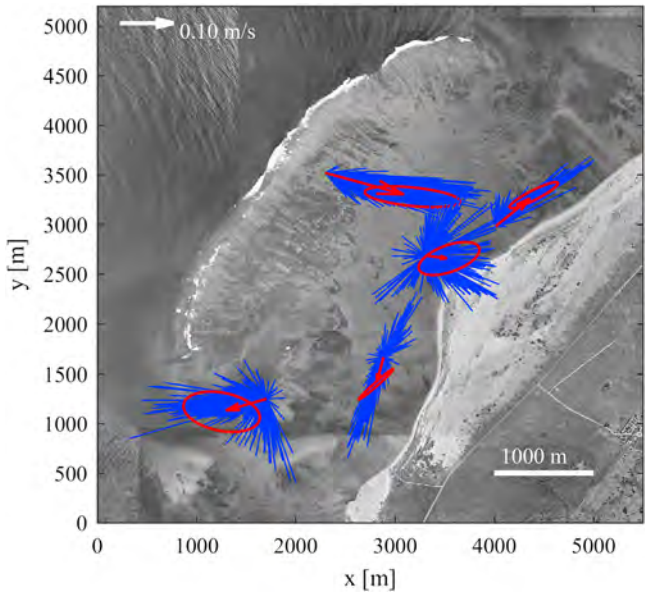

Figure 4. Hourly mean depth-averaged current data (blue), with the experiment-averaged mean current vector indicated by the arrows. The ellipses (red) indicate the direction of the major and minor semi-axes of variability. The scale of the ellipse represents one standard deviation.

The EOF analysis revealed two distinct flow patterns in the subtidal (low-pass filtered) component of the currents (Figure 5a). The first flow pathway (mode 1, accounting for ~95% of the current variability) was directed across the reef flat and toward the salient where it diverged symmetrically near the salient and returned to the ocean via the two channels (red vectors in Figure 5a); this pattern was also consistent with the magnitude and direction of the experiment-averaged current vectors in Figure 4 and the paths of the Lagrangian drifters (Figure 5d). The EOF amplitude time series indicated that this pathway was prevalent throughout most of the experiment and intensified during the swell events (Figure 5b). The fore reef $H_{m0,sw}$ (Figure 5c) was strongly correlated (R^2 = 0.90) with this first mode (maximum correlation at zero phase lag). The second flow pathway (mode 2) identified by the EOF analysis of the subtidal velocities (blue vectors in Figure 5a) was directed northward along the shoreline. However, for much time this mode was insignificant except at both the start and end of the experiment (Figure 5b). For this mode to dominate, the fore reef wave heights needed to be small ($\lesssim$1 m) so that the wave-driven flows were weak, and the alongshore component of the wind $\gtrsim$3.8 m/s. Early in the experiment (prior to 2 August) as well as later in the experiment (8–9 August), these conditions occurred (Figure 5c). It was during these later conditions that the drifters also measured a consistent northward flow (Figure 5e).

The intratidal current variability could also be mostly described by two primary flow patterns. The first flow pattern (mode 1), which accounted for ~54% of the intratidal current variability, was directed through the channel and northward within the lagoon (Figure 6a); little cross-reef flow was associated with this flow pattern. The mode 1 amplitude (Figure 6b) was predominantly associated with the tide (R^2 = 0.90) and led the tidal surface elevation (Figure 6c) by 3 hr. This tidal contribution thus caused the currents to vary about the mean flow at S5 by ~0.08 m/s. The second flow pattern (Figure 6a; mode 2 accounting for ~17% of the intratidal variability) was directed across the reef flat and channel and along the shoreline. The amplitude of this mode was negatively correlated with the tidal surface elevation (Figure 6c; R^2 = 0.64); the magnitude of the flow was highest at low water depths and decreased as the water depth on the reef flat increased. This mode describes the response of the tidal modulation of the wave-driven currents. During low tide, the current is enhanced across the reef (by up to ~0.04 m/s) and along the shoreline to the south (by up to ~0.03 m/s) but is reduced in the southern channel (by up to ~0.03 m/s). In contrast, during high-tide conditions, the mean current was reduced across the reef and along the shoreline (by up to ~0.04 and ~0.02 m/s, respectively) but slightly enhanced in the southern channel (by up to ~0.04 m/s).

3.4. Bed Shear Stresses

The experiment-averaged (denoted by the overbar) mean bed shear velocity ($\overline{u_{*m}}$) for the combined wave-current conditions was greatest on the reef flat at S2 and substantially smaller in the lagoon at S5 (~60% of the $\overline{u_{*m}}$ measured at S2; Figure 7a). North and south of the salient at S8 and S9, $\overline{u_{*m}}$ was slightly larger than at S5 despite these sites being located at a similar distance from the shoreline and at similar depths. The $\overline{u_{*m}}$ in the southern channel at S7 was also smaller than at S2 but was slightly higher than the other lagoon stations. The maximum shear velocities averaged over the entire experiment $\overline{u_{*max}}$ (Figure 7b) exhibited a similar spatial distribution, with the exception that the value at S7 was slightly larger than S2.

When the offshore waves were small ($H_{m0,sw} \lesssim$ 1 m), u_{*m} tended to be similar in magnitude at all sites but variable in time, especially at S8 and S9. During the swell events when the waves offshore were larger ($H_{m0,sw} \approx$ 2 m), u_{*m} increased in magnitude at all sites and tended to vary at intratidal timescales. During these swell events, u_{*m} on the reef flat at S2 was comparable to the southern channel at S7 (both ranging from 0.014 to 0.016 m/s), but values were on average approximately two times smaller at S5 (0.008 m/s; Figures 7c and 7d) and slightly larger than at both S8 (0.012 m/s) and S9 (0.011 m/s; Figures 7e–7g). The maximum friction velocities associated with the infragravity waves $\left(u_{*max,ig}\right)$ on average ranged between 0.016 and 0.019 m/s across all sites and thus tended to be larger than u_{*m}.

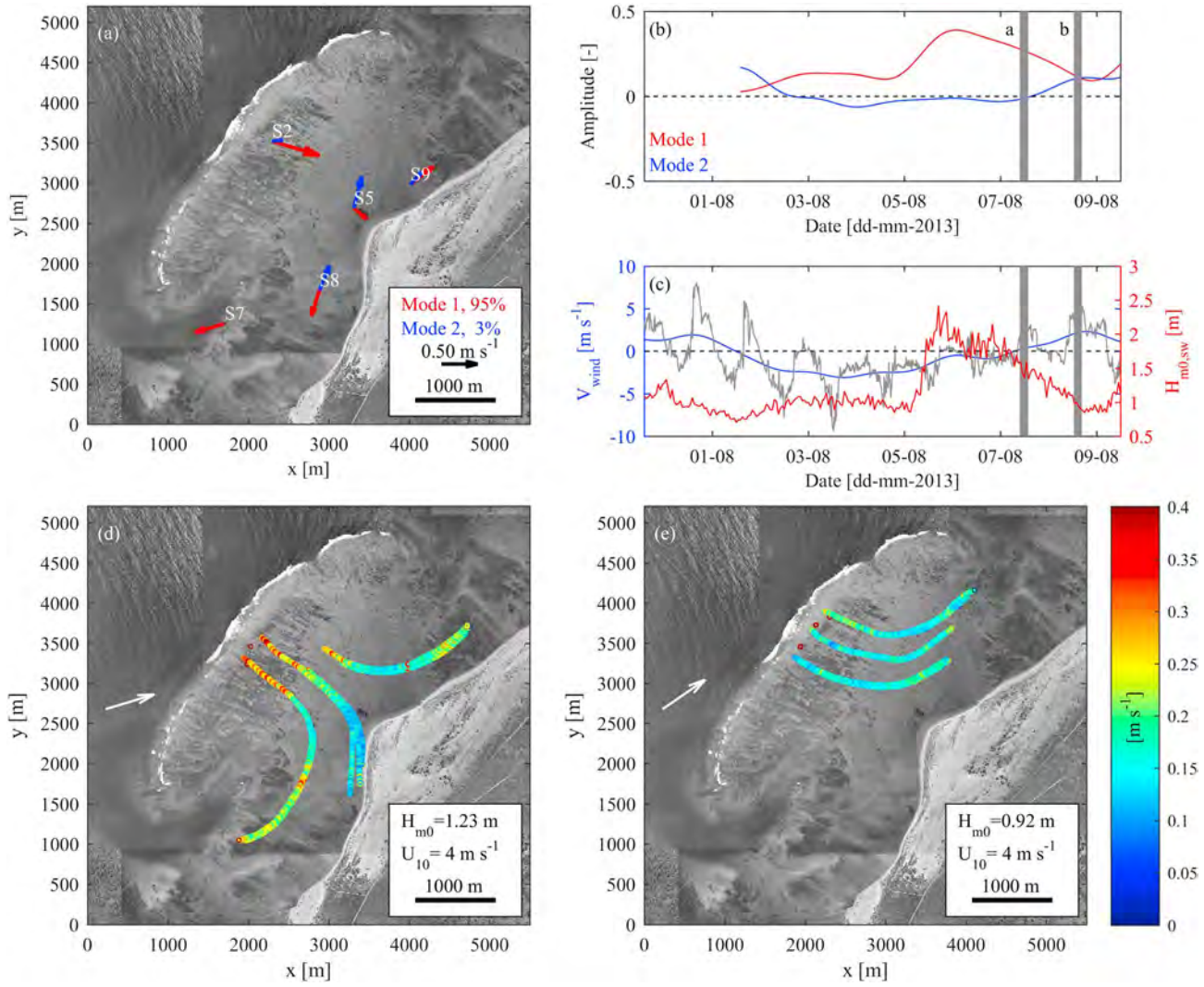

Figure 5. (a) The first (red) and second (blue) 36-hr empirical mode of subtidal current variability along with (b) the amplitude of the first (red) and second (blue) modal amplitude time series from the empirical orthogonal function analysis. To facilitate comparison of the two modes, the amplitude of the arrows and amplitude time series have been scaled (factor = 0.64) so that the arrows are equal in magnitude at S8. (c) The alongshore wind speed V_{wind} averaged over 10 min (gray) and at subtidal temporal scales (blue). The fore reef sea-swell wave height ($H_{m0,sw}$) is shown in red. The gray shading indicates the drifter experiments shown in (d) that started at 09:32 on 7 August 2013 and (e) that started at 12:40 on 8 August 2013. (d–e) Surface current Lagrangian drifter trajectories measured for different forcing and tidal states (indicated in Figure 2). The white arrow denotes the wind direction. The velocity of the drifters is indicated by the color of the drifter track and described by the colorbar (in m/s).

The sea-swell waves made the largest contribution to the bed shear velocities at all sites ($u_{*max,sw}$ values averaged at S2 = 0.020 m/s, S5 = 0.011 m/s, S7 = 0.025 m/s, S8 = 0.015 m/s, and S9 = 0.016 m/s). At S2, $u_{*max,sw}$ varied at intratidal timescales due to the tidal modulation of reef flat wave heights, with only a slight increase observed during the two swell events at all stations (particularly prevalent at S7). During high tide, the $u_{*max,sw}$ at S2 was approximately two times greater than at S5, whereas at low tide conditions, it was only ~40% greater. The $u_{*max,sw}$ was largest at S7 and was similar in magnitude to that at S2 when the waves were small but was approximately 1.5–2 times greater than at S2 during the swell events.

3.5. Suspended Sediment Concentrations

Early in the experiment when the waves were small (1–6 August; Figure 8a), the SSCs on the reef flat at S2 varied from ~0.5 mg/L at low tide to ~2–3 mg/L at high tide (Figure 8c). During the swell events (6–8 and 9–12 August), the SSCs at S2 were consistently higher and peaked at ~8 mg/L but also varied with the

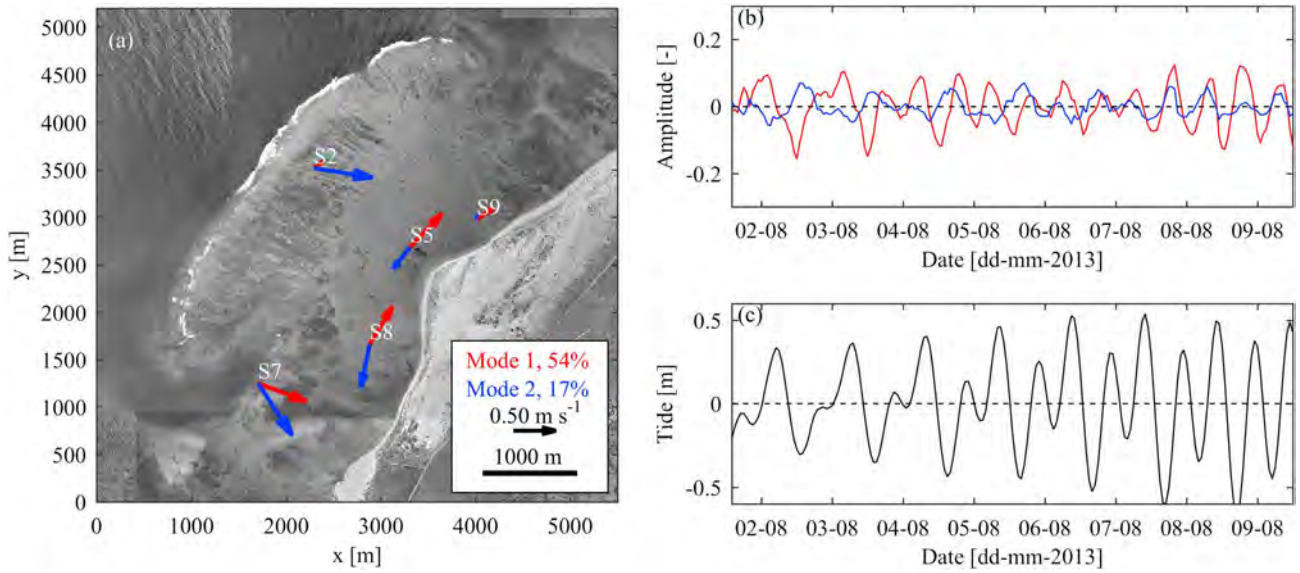

Figure 6. (a) The first (red) and second (blue) empirical model intratidal current variability, along with (b) the respective modal amplitude time series. To facilitate comparison of the two modes, the amplitude of the arrows and amplitude time series have been scaled (factor = 1.18) so that the arrows are equal in magnitude at S8. (c) The tidal variation measured on the fore reef.

tide. In contrast, in the lagoon near the tip of the salient (S5), the SSCs tended to be approximately twice as large and ranged from ~2 mg/L in low swell conditions to ~4–20 mg/L during the swell events (Figure 8d). Similar to the reef flat observations, the SSCs were substantially influenced by the sea-swell offshore wave conditions and were also strongly tidally modulated. The temporal decomposition of the SSC time series at S2 from the singular-spectrum analysis revealed that ~85% of the variance in SSC (Figure 8e) was described by subtidal variability. A further ~9% of the SSC variance occurred at intratidal timescales (Figure 8e). Similar modes of SSC variability were also measured near the salient at S5, where ~95% of the variability was explained by two modes and consisted of a dominant subtidal mode (~79% of SSC variability; Figure 8f) and an intratidal mode (~15% of SSC variability).

When the waves in the channels were small ($H_{m0,sw} \lesssim 0.5$ m), the SSCs measured in the southern channel (S7) ranged from ~3 mg/L at low tide to ~5 mg/L at high tide (Figure 9c). However, during the swell events when the waves were larger ($H_{m0,sw} \approx 1.5$ m; Figure 9a), the SSC was substantially greater, with a peak hourly mean SSC of ~80 mg/L. This was an order of magnitude greater than the values observed on the reef flat at S2 and approximately four times greater than that measured at S5. A similar pattern in the SSC variability was also measured in the northern channel (S10), albeit the magnitudes were smaller (Figure 9d). At both channel locations, the measurements were obtained slightly higher above the bed than at the locations on the reef flat and the lagoon; hence, if anything, they would also be underestimating the true near-bed SSC at these locations. Most of the SSC variability in the channels occurred at subtidal timescales (81–91%; mode 1 in Figures 9e and 9f). During the swell events, the SSCs displayed much greater intratidal variability (particularly at S7); however, this variability only accounted for ~8% of the total SSC variability at S7 (mode 2 in Figure 9e).

3.6. Relationship Between Bed Shear Stresses and SSC

Conventional sediment transport formulations describe SSC function of bed shear stresses and sediment properties. In a fringing coral reef environment, where the morphology of the reef strongly influences the hydrodynamic processes (waves, currents, and water levels) within the nearshore zone, the individual contributions of sea-swell waves, infragravity waves, and mean currents to the SSC variability is still not well established but can be expected to contribute to the stress imposed on the bed (equation (8)):

$$\mathrm{SSC} = f(u_*) = f\left(u_{*max,sw}; u_{*max,ig}; u_{*m}\right) \tag{8}$$

To assess the relative importance of these hydrodynamic processes to SSC variability, the individual bed shear velocity contributions were evaluated against the SSC by stepwise multiple regression analysis. In

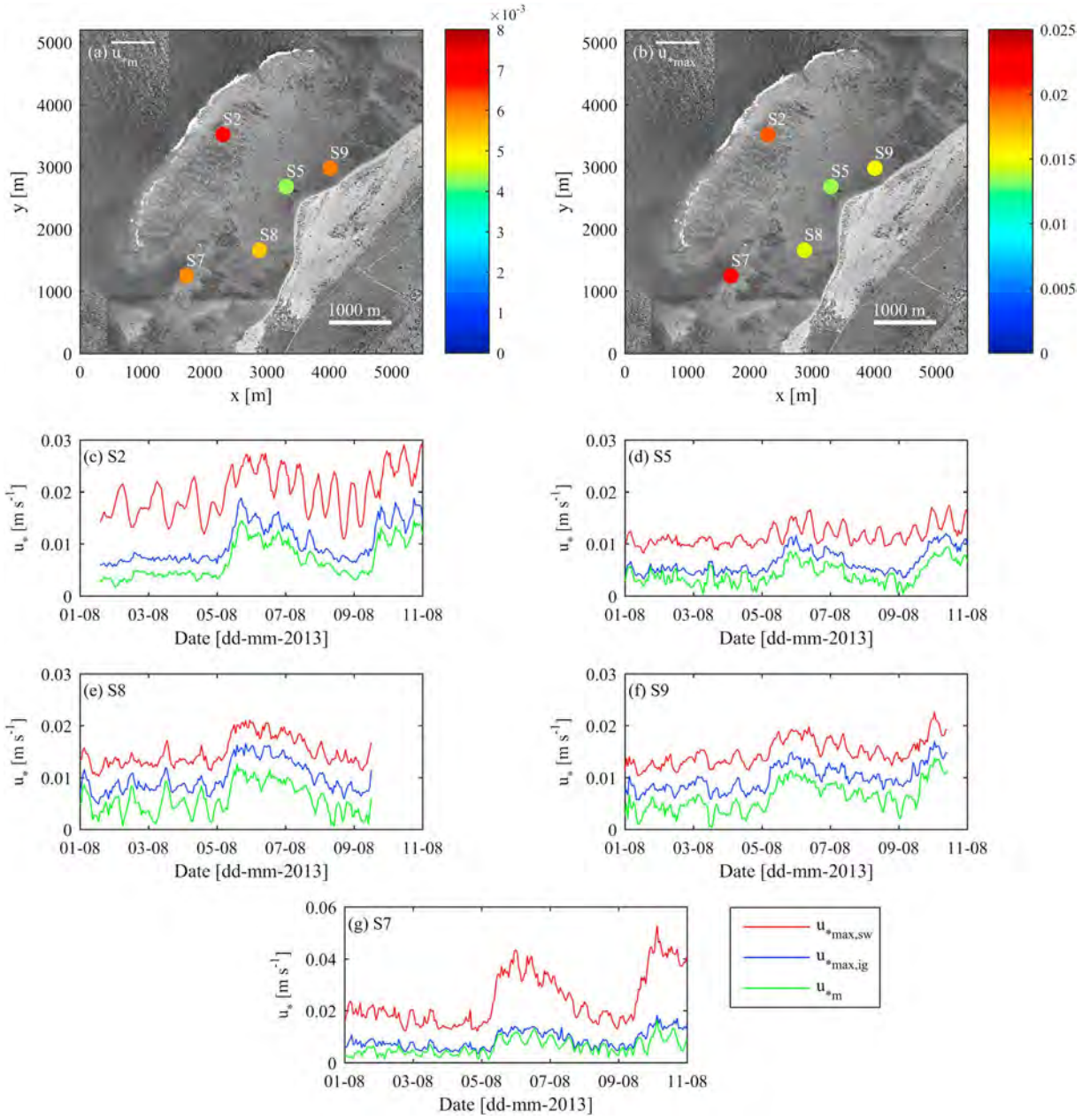

Figure 7. The experiment averaged near the bed (a) mean wave-current shear velocity $\overline{u_{*m}}$ and the (b) maximum wave-current shear velocity $\overline{u_{*max}}$. The colorbars (with different scales) denote the shear velocities in m/s. The shear velocities near the bed (c) on the reef flat at S2, (d) in the lagoon near the tip of the salient at S5, (e) south of the salient at S8, (f) north of the salient at S9, and (g) in the southern channel at S7, generated by sea-swell wave-current conditions $u_{*max,sw}$, infragravity wave-current conditions $u_{*max,ig}$, and the mean currents (u_{*m}). Note the different vertical scale used in (g).

this way, we can assess how the inclusion of different shear stress contributions improves predictions of the SSC variability.

The analysis indicated that $u_{*max,sw}$ on the reef flat (S2), in the lagoon (S5), and in the southern channel (S7) was much stronger correlated with the SSC than $u_{*max,ig}$ and u_{*m} (Table 4). There was some slight improvement in the correlation when $u_{*max,ig}$ and u_{*m} were considered; however, this improvement (despite being statistically significant) was small (e.g., 0.63 versus 0.66 at S2, 0.56 versus 0.60 at S5 and 0.69 versus 0.76 at S7). Thus, sea-swell waves were the key driver of the total SSC variability throughout the fringing coral reef and lagoon system while infragravity waves and mean currents appeared to make a secondary contribution to the SSC variability.

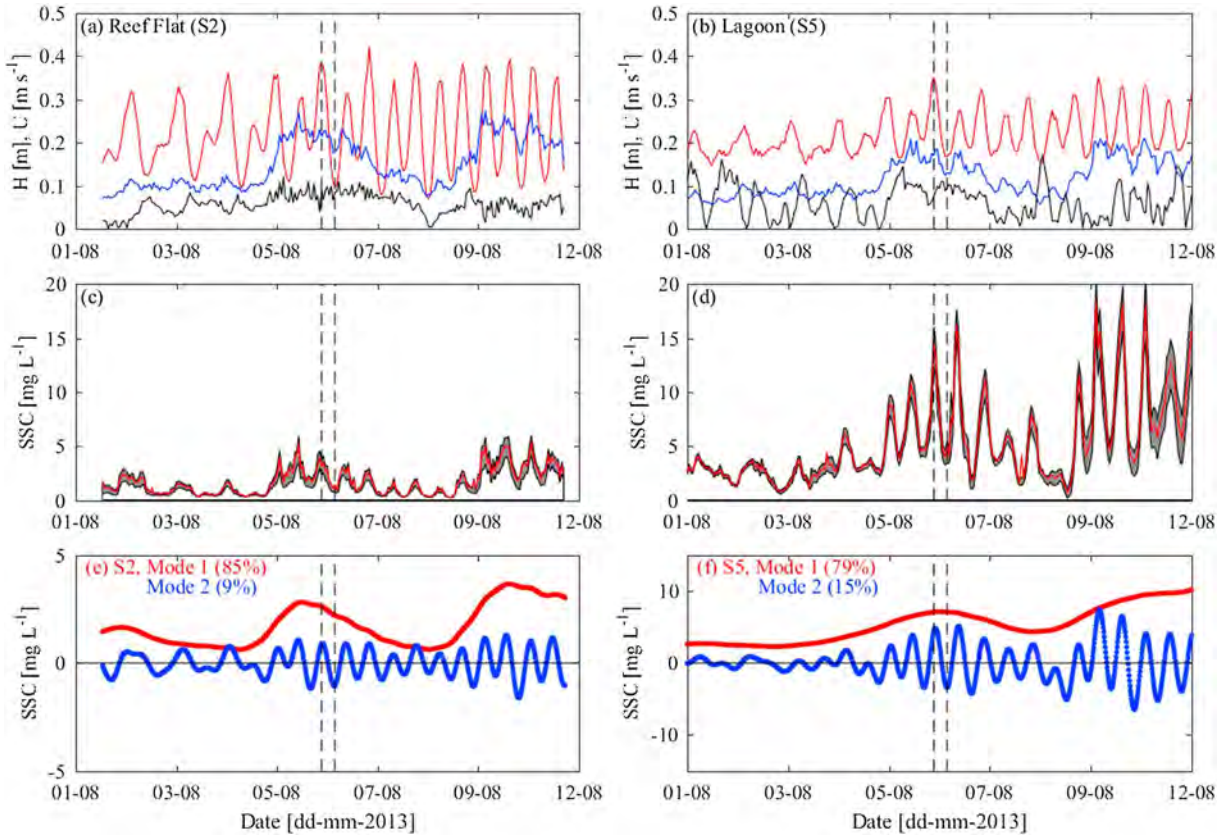

Figure 8. Sea-swell ($H_{m0,sw}$, red) and infragravity ($H_{m0,ig}$, blue) wave forcing and the absolute current (U, black) (a) on the reef flat at S2 and (b) in the lagoon at S5. Hourly mean SSCs are shown in red (c) on the reef flat at S2 and (d) in the lagoon at S5. The lower limit represents the first quartile while the upper limit indicates the third quartile for each hourly burst of data. The bottom row shows the decomposed SSC time series indicating the first (red) and second (blue) modes, which explained the majority of the signal variance, at (e) S2 and (f) S5. The vertical dashed lines indicate a high and low tide.

4. Discussion

A number of prior studies have observed SSC variability in both space and time across a wide range of reefs in the Caribbean (e.g., Hubbard, 1986), the Pacific Ocean (e.g., Ogston et al., 2004; Presto et al., 2006; Storlazzi et al., 2004; Vila-Concejo et al., 2014), and the Indian Ocean (e.g., Morgan & Kench, 2014; Pomeroy et al., 2017). However, these studies have not focused specifically on how different hydrodynamic mechanisms contribute to driving spatial patterns in SSCs and pathways across different zones of a fringing coral reef-lagoon system as the relative importance of these different hydrodynamic processes change.

The SSC differences observed at different locations within the fringing coral reef-lagoon system were strongly influenced by variability in the local hydrodynamic conditions. For example, the high SSCs observed in the channels (Figure 9) can be explained by the propagation of much larger waves into the channels, as well as the enhancement of mean flows that converge in these channels (Figures 3 and 4), whereas the low concentrations on the reef flat and in the lagoon can be explained by the smaller waves that propagate over the reef flat into the lagoon and reduction in cross-reef currents. This reduction in wave height and cross-reef currents has been observed in numerous field studies, which have demonstrated that this reduction is due to wave breaking as well as bottom friction due to the presence of large bottom roughness on the reef flat (e.g., Lowe, Falter, et al., 2005). In reef systems, this dissipation of incident energy also typically results in a bimodal wave spectrum and infragravity wave heights that are comparable to the sea-swell wave heights in back reef/lagoon regions (Brander et al., 2004; Hardy & Young, 1996; Harris et al., 2014; Lugo-Fernández et al., 1998; Pomeroy et al., 2012; including at the present study site). While infragravity waves have been found to play an important role in beach erosion (e.g., van Thiel de Vries et al., 2008), in the cross-shore transport of sediment by nonlinear waves (e.g., de de Bakker et al., 2014) and shoreline run-up on reef fringed islands (e.g., Cheriton et al., 2016), in the present study the bed shear stresses associated with infragravity waves were

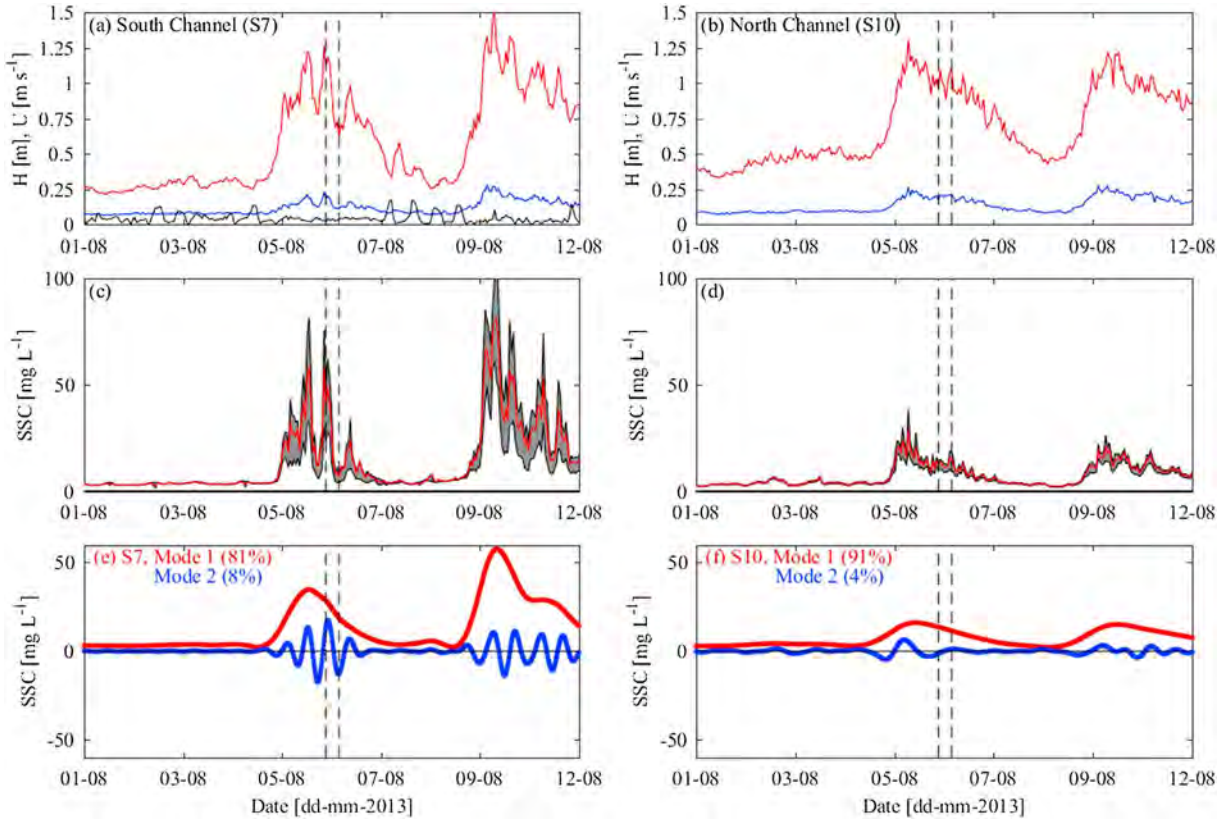

Figure 9. Sea-swell ($H_{m0,sw}$, red) and infragravity ($H_{m0,ig}$, blue) wave forcing and the absolute current (U, black) (a) in the south channel S7 and (b) in the north channel at S10. *Note*: The current was not measured in the S10. Hourly mean SSCs are shown in red (c) in the south channel at S7 and (d) in the north channel at S10. The lower limit represents the first quartile while the upper limit indicates the third quartile for each hourly burst of data. The bottom row shows the decomposed SSC time series indicating the first (red) and second (blue) modes, which explained the majority of the signal variance, at (e) S7 and (f) S10. The vertical dashed lines indicate a high and low tide.

of secondary importance (e.g., Figure 7) to the sea-swell waves throughout the fringing coral reef-lagoon system (reef flat, lagoon, and channels). This is due to the much longer wave periods and the smaller wave friction factors associated with infragravity waves (Lowe, Falter, et al., 2005); therefore, infragravity waves make a much smaller contribution to the bed shear stresses for the same wave height. Mean currents were also of secondary importance. This is consistent with the wave-dominated hydrodynamics not only observed at this site but also at other analogous reefs (e.g., Taebi et al., 2011). For these reefs, mean currents generated by wave breaking on fore reef and reef crest are stronger than those associated with the propagation of the tide, which only modulate the mean current intratidal timescales. In contrast, for reef systems that are tidally dominated, SSC variability has instead been shown to be strongly correlated with the propagation of the tide (e.g., Hoitink, 2004).

Table 4
The Correlation (R^2) Between Bed Shear Velocities and the Total Suspended Sediment Concentrations Measured on the Reef Flat (S2), in the Lagoon (S5), and in the Southern Channel (S7)

	S2	S5	S7
$u_{*max,sw}$	0.63	0.56	0.69
$u_{*max,ig}$	0.40	0.51	0.55
u_{*m}	0.40	0.40	0.49
$u_{*max,sw} + u_{*max,ig} + u_{*m}$	0.66	0.60	0.76

Note. The shear velocities are decomposed according to the mean stress (u_{*m}), and the stresses due to the infragravity waves $(u_{*max,ig})$ and sea-swell waves $(u_{*max,sw})$. For all cases $p < 0.05$.

While the spatial differences in SSC can be explained by the local hydrodynamic forcing, this forcing alone could not explain all of the spatial variability in the SSC, with a notable example being the difference in the magnitude of the SSCs where they were greater in the lagoon near the salient (S5) when compared to the reef flat (S2; Figure 8). This difference in SSC is important because there was less energy at S5 (i.e., the wave and current bed stresses were smaller), and thus, it would be expected that the SSCs would also be lower (e.g., Brander et al., 2004). The subsequent discussion will focus on three possible explanations for this spatial variability before a conceptual model that synthesizes the results of this study is presented in section 4.4.

4.1. Bed Shear Stress Variability

If the observed increase in SSC in the lagoon was driven by local sediment resuspension, it would be expected that the bed shear velocities would be larger in the lagoon at S5 than on the reef at S2 (we note that grain size and availability will also have an impact, which is addressed later). Such a difference in bed stress could also be expected as the waves propagate across the reef flat and dissipate due to the presence of the large bottom roughness. This roughness also vertically attenuates the current- and wave-orbital-driven flows within the roughness, which reduces the shear velocities near the bed when compared to a bare bed (e.g., Le Bouteiller & Venditti, 2015; Lowe et al., 2008; Lowe, Koseff, et al., 2005; Luhar et al., 2010; Stocking et al., 2016). This was previously demonstrated on the reef flat (S2) at this site in Pomeroy et al. (2017), where it was shown that the total resistance exerted on the overlying flow (τ_{total}) did not represent the actual bed shear stresses (τ_{bed}) imparted on the underlying sediment at the base of the immobile roughness (canopies). However, despite this demonstrated reduction on the reef flat, the computed bed shear velocities were still greater at S2 than at S5, the opposite of the observed SSC trend (Figure 7). Thus, the results indicate that spatial differences in the bed shear stress in the lagoon cannot explain the difference in the SSC magnitude between the reef flat and the lagoon.

4.2. Sediment Advection

Another possible explanation for the difference in SSC magnitude between the reef flat and the lagoon could be the advection of sediment from the reef flat toward the shoreline that may supplement locally suspended sediment. However, the Lagrangian drifter measurements and the flow patterns identified by the EOF analysis indicate that the flow that transports suspended sediment within the lagoon does not converge at the salient (Figure 5). The mean flow pathway spatially diverges toward the channels and hence so too must the suspended sediment advected by this flow. In addition to this divergence, these measurements also indicate that the mean current decreased in magnitude from the reef crest to the shoreline (Figures 3 and 4); therefore, the time available for sediment to settle out of the water column would increase shoreward over the reef flat.

If it is assumed that the sediment suspended on the reef flat ranges from 50 to 500 μm at a density of 2,600 kg/m^3, it would take these grains ~40 to 1,650 s to settle through the roughly ~3-m lagoon water depth and, based on the Eulerian and Lagrangian measurements of the mean currents, thus could travel only ~15–500 m before the sediment is deposited on the seabed. The distance between the back of the reef flat and the salient is ~1,200 m. The reduced $u_{*max,sw}$ behind the reef flat may then resuspend a finer fraction of this sediment, but the larger grains that could be suspended on the reef flat may not be resuspended within the lagoon; at S5 the shear velocity is smaller (Figure 7d). As a consequence, there would likely be a reduction in the original sediment advected from the reef flat that can be resuspended landward across the lagoon so the SSC would also be expected to decrease. Therefore, advection does not appear to be a likely cause of these spatial differences.

4.3. Sediment Availability Across Different Reef Zones

By excluding differences in bed shear stresses and sediment advection as the primary causes of the SSC discrepancy between the reef flat and the lagoon, another explanation for the reduced SSC on the reef could be the differences in variations in seabed sediment characteristics and availability. The issue of the availability of sediment for suspension can be separated into two components: (1) the availability of sediment of a *suitable size* for suspension and (2) the *volume* of that suitably sized sediment on the reef flat for suspension and transport (note that there is negligible terrestrial input at this site).

The sediment on the reef flat is coarser than the sediment in the lagoon (Figure 10a). Such trends in median grain size have also been commonly observed across a number of different reef environments (e.g., Cordier et al., 2012; Harris et al., 2014; Morgan & Kench, 2014). The absence of finer-grained sediment suggests that at this site, sediment is continually transported off the reef flat into the lagoon, with some sediment likely to exit via the channels; the suspension of sediment of a suitable grain size is source limited, rather than limited by shear stress (the shear stresses are sufficient to suspend the sediment). This also demonstrates that the use of sediment transport descriptors that rely on the median grain size (D_{50}) to describe sediment transport are likely to incorrectly estimate the SSC in these environments. This can also demonstrated by comparing the relationship between u_{*max} and SSC at S2 (Figure 10b), which indicates that despite the wide range of

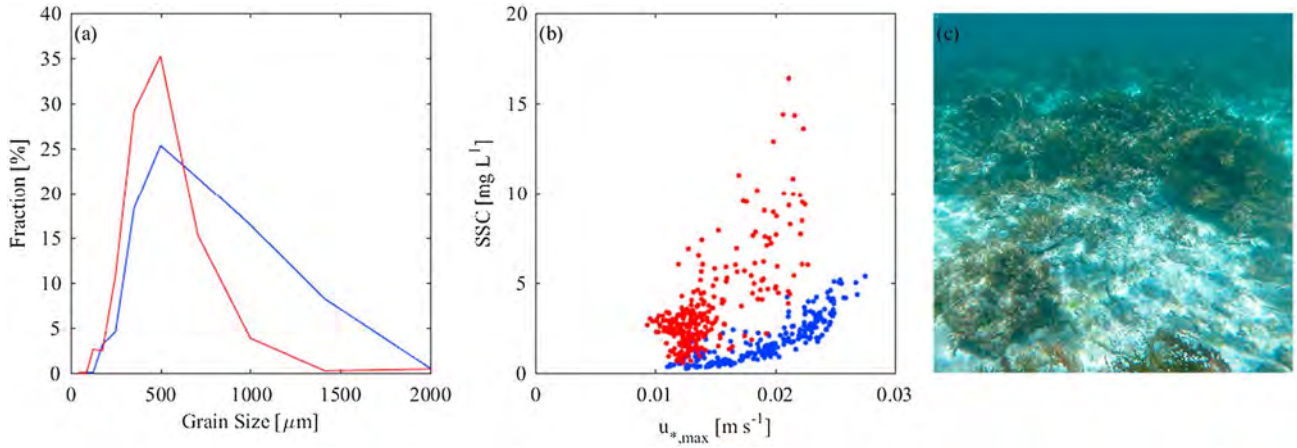

Figure 10. (a) The grain size distribution on the (blue) reef flat at S2 and (red) near the salient at S5. (b) The relationship between hourly mean SSC and the hourly mean maximum shear velocity near the bed (u_{*max}) at (blue) S2 and (red) S5. (c) An underwater image typical of the benthos of the reef flat.

shear velocities experienced at S2, the values of SSC remain low. In the lagoon, where the sediment distribution contains finer-grain particles than on the reef flat, there is more sediment of a suitable size available for suspension. Thus, despite the lower magnitude of u_{*max} at S5, the SSC would be expected to be greater when compared to S2 (Figure 10b), which is supported by the measurements.

In addition, conventional sediment transport predictions also assume a bed is fully occupied by sediment of unlimited supply, which is clearly not the case on many coral reefs, including on the reef flat (i.e., at S2). At S2, bed sediment is interspersed between roughness elements that may occupy a large proportion of the planform area, thereby reducing the area over which the sediment can be entrained (Figure 10c). Furthermore, these large roughness elements are often fixed to hard pavement not far below the surface of the sediment. Although this experiment did not precisely quantify the volume of sediment available for transport on the reef flat, the presence of large roughness clearly reduces the planform area from which sediment can be suspended (sand and rubble only account for 5–30% of the bed on the reef flat; Cuttler et al., 2015) when compared to the adjacent sandy lagoon where sand could be up to 80% of the benthic composition. Thus, irrespective of the sediment grain size distribution, there can be limited sediment available for suspension on the reef flat.

4.4. Synthesis: Mechanisms of Suspension and Pathways of Transport Across Fringing Coral Reef-Lagoon Systems

A conceptual model (Figure 11) has been proposed that describes the sediment transport in a wave-driven fringing coral reef broken by channels in the reef. In this model, large sea-swell waves break in the narrow surf zone region near the reef crest (Figure 11a). The extent of wave breaking depends on the offshore wave height (varying over subtidal timescales) and tidal variations in the reef flat water depth. This variability in wave breaking is analogous to the spatial variability observed on barred beaches, where waves break over shallow sandbars; however, for reefs the fore reef slope is often steeper and thus the width of the surf zone narrower and located much further from shore. Cross-reef wave-driven currents are also affected by the variation in the water depth and thus vary over subtidal and intratidal timescales. At high tidal elevations, large swell waves propagate over the reef flat, but as the tidal water depth decreases, more swell wave energy is dissipated by wave breaking. This leads to intratidal variability in the forcing that entrains some sediment from the seabed (e.g., Figures 8 and 9). As the water depth decreases and during swell events, the relative magnitude of cross-reef currents increase and infragravity waves make an increasing contribution to the total wave height across the reef flat (e.g., Figure 3). The increase in the cross-reef currents and infragravity waves does not result in these shear stresses becoming the dominant stress imposed on the sediment but does contribute to enhancing the overall bed shear stresses, particularly during swell events (e.g., Figure 7). On the reef flat, the presence of large immobile bottom roughness that occupies a substantial fraction of the plan area can reduce the shear stresses imposed on bed sediment when compared to a seabed without roughness and limit the volume of sediment available for suspension into the water column.

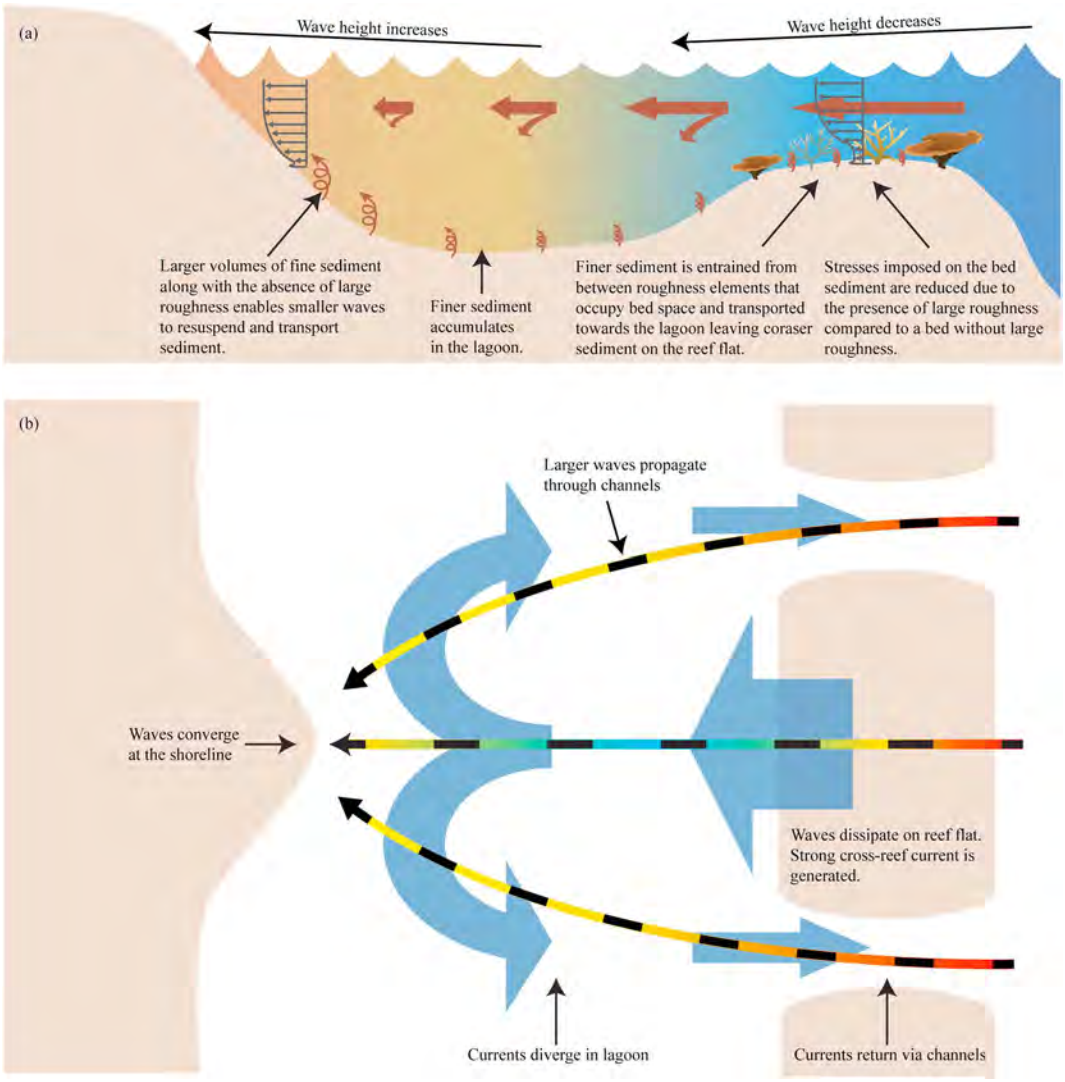

Figure 11. Conceptual model of sediment transport processes in a fringing coral reef-lagoon system. (a) Cross section of waves, currents, and sediment processes across a reef and lagoon. Brown arrows indicate the direction of sediment transport by currents, and the upward arrows indicate sediment resuspension. Note that an increase in suspended sediment concentration is indicated by brown shading. (b) Plan view of the wave rays (colored lines) and current pathways (solid blue arrows) throughout a reef system. The color gradient indicates the change in wave height (red corresponds to larger waves and blue to smaller waves).

Furthermore, the continual transport of sediment (due to the high energy environment that prevents the deposition of the sediment) across the reef flat into the lagoon results in relatively low quantities of sediment of a suitable size available for suspension into the water column.

Within the lagoon (Figure 11b), the waves and currents decrease in magnitude. However, waves propagating through the channels refract into the lagoon and increase the wave height close to the shoreline (e.g., Figure 3). The reduced bottom roughness and greater availability of finer sediment generate more sediment entrainment and higher SSCs in the lagoon (in particular close to the shoreline). Sediment that is suspended within the lagoon is transported by shoreward-directed currents that diverge near the shoreline, converge, and increase in magnitude in the channels and exit through the channels as a relatively strong narrow offshore-directed current (e.g., Figure 5), thus also similar to the rip currents that form on barred beaches (e.g., Dalrymple et al., 2011). Overall, there are many similarities in the circulation patterns in the dynamics of fringing reefs when compared to rip currents on barred beach with the main difference being the scale of the respective systems: rip currents on barred beaches tend to be O10–100 m while fringing reefs are O100–1,000 m.

For wave-driven fringing coral reef systems, such as the site considered in this study, the proposed model describes how hydrodynamic processes would be expected to transport sediment under a range of wave conditions. While this model suggests that suspended sediment will be transported to toward the channels by diverging cross-reef currents, there of course may be exceptions where this does not occur; for example, under favorable alongshore wind conditions, sediment transport may predominantly be in one direction (in this experiment, to the north). Furthermore, this model may breakdown under extreme conditions (e.g., tropical cyclones), when the sediment transport processes may be highly storm dependent.

5. Conclusions

In this study, we investigated the physical process contribution and relative importance of sea-swell, infragravity waves, mean currents to the spatial, and temporal variability of SSCs.

The key results of this study are as follows:

1. In two-dimensional fringing reef-lagoon environments with gaps/channels in the reef crest and reef flat, sea-swell wave heights within the lagoon can be enhanced relative to the waves that propagate across the back region of reef flat due to the propagation and diffraction of waves through the channels. The height of these waves in the channels is related to the offshore wave conditions due to the greater depth.
2. The mean flow within a microtidal fringing reef system is predominantly driven by subtidal variations in the offshore sea-swell wave conditions; however, when the offshore waves are small and alongshore winds are strong and persistent, flows can occasionally be driven directly by the wind. In addition to the subtidal variability, flow within the lagoon also varies at intratidal timescales. This variability in the alongshore direction is driven by the propagation of the tidal flow through the lagoon while variability in the cross-shore direction is due to a tidal modulation of wave-driven flows.
3. On the reef flat, in the lagoon, as well as in the channels, sea-swell waves make the primary contribution to the bed shear stresses that drive sediment resuspension. Infragravity waves and currents also make a statistically significant contribution to the bed shear stress, but this contribution is comparatively small.
4. On reef flats where a significant percentage of the bed is occupied by immobile roughness elements such as corals, cor-algal ridges, and pavements, less sediment is available for transport, and the sediment that is available is coarser than the sediment in the lagoon. The increased availability of finer-grained sediment in the lagoon results in larger SSCs in the lagoon than on the reef flat where the shear stress imposed on the bed sediment is higher. It is unclear, however, if these spatial differences in concentrations are observed in all reef systems. However, the continual cross-reef transport of finer-grained sediment due to wave breaking on the reef flat combined with wave-driven flow is likely to result in only coarser sediment grains remaining on the reef flat in many systems and an accumulation of finer sediment in lagoons that are more easily suspended than those on the reef flat.
5. For many fringing reef-lagoon systems, the majority of the SSC variability will occur over subtidal timescales, which is related to the arrival of larger sea-swell waves to the site. Such subtidal variation is also associated with storms, which are known to be both constructive and destructive to coral reefs and their morphology. When evaluating the resilience of ecosystems to elevated SSC, subtidal variability may be more important to understand than shorter duration variations in SSC such as those that occur at intratidal timescales, especially given that most tropical coral reef systems worldwide are more strongly forced by variability in sea-swell waves than tides (Lowe & Falter, 2015).

Acknowledgments

A. W. P. is grateful for the support of a Robert and Maude Gledden Postgraduate Research Award and by The Gowrie Trust Fund (2013, 2014). G. W. acknowledges the support of an International Postgraduate Research Scholarship, an Australian Postgraduate Award, and an EA and CH Jenkins scholarship. M. C. acknowledges the support of a Scholarship for International Research Fees and a University International Stipend. This project was funded by the Western Australia Marine Science Institute (WAMSI) Dredging Science Node (Theme 2/3), an Australian Research Council Future Fellowship (FT110100201), and an Australian Research Council Discovery Project grant (DP140102026) to R. J. L., as well as the U.S. Geological Survey Coastal and Marine Geology Program. The authors thank Sana Dandan, Jim Falter, Jeff Hansen, Malcolm McCulloch, and Leonardo Ruiz Montoya for their assistance during the experiment. We thank Mark Buckley, Ana Vila-Concejo, Daniel Harris, and Javier Leon who reviewed this manuscript. Data sets analyzed in this manuscript are available from http://doi.org/10.5281/zenodo.126670.

References

Acevedo, R., Morelock, J., & Olivieri, R. A. (1989). Modification of coral reef zonation by terrigenous sediment stress. *PALAIOS*, *4*(1), 92–100. https://doi.org/10.2307/3514736

Anthony, K. (2000). Enhanced particle-feeding capacity of corals on turbid reefs (Great Barrier Reef, Australia). *Coral Reefs*, *19*(1), 59–67. https://doi.org/10.1007/s003380050227

Australian Institute of Marine Science. (2013). AIMS Ningaloo Reef Platform. Retrieved November 13, 2014, from http://data.aims.gov.au/aimsrtds

Bagnold, R. A. (1966). An approach to the sediment transport problem from general physics. *US Geol. Surv. Prof.* Pap., 422–I, I1–I37.

Beardsley, R. C., Limeburner, R., & Rosenfeld, L. K. (1985). Introduction to the CODE-2 moored array and large-scale data report. CODE-2: Moored Array and Large-Scale Data Report, 85–35.

Bosman, J. J., van der Velden, E. T. J. M., & Hulsbergen, C. H. (1987). Sediment concentration measurement by transverse suction. *Coastal Engineering*, *11*(4), 353–370. https://doi.org/10.1016/0378-3839(87)90033-0

Brander, R. W., Kench, P. S., & Hart, D. (2004). Spatial and temporal variations in wave characteristics across a reef platform, Warraber Island, Torres Strait, Australia. *Marine Geology*, *207*(1–4), 169–1-4. https://doi.org/10.1016/j.margeo.2004.03.014, 184

Buddemeier, R., & Hopley, D. (1988). Turn-ons and turn-offs: Causes and mechanisms of the initiation and termination of coral reef growth. Lawrence Livermore National Lab., Livermore, CA.

Chave, K. E., Smith, S. V., & Roy, K. J. (1972). Carbonate production by coral reefs. *Marine Geology*, *12*(2), 123–140. https://doi.org/10.1016/0025-3227(72)90024-2

Cheriton, O. M., Storlazzi, C. D., & Rosenberger, K. J. (2016). Observations of wave transformation over a fringing coral reef and the importance of low-frequency waves and offshore water levels to runup, overwash, and coastal flooding. *Journal of Geophysical Research: Oceans*, *121*, 3121–3140. https://doi.org/10.1002/2015JC011231

Cordier, E., Poizot, E., & Méar, Y. (2012). Swell impact on reef sedimentary processes: A case study of the La Reunion fringing reef. *Sedimentology*, *59*(7), 2004–2023. https://doi.org/10.1111/j.1365-3091.2012.01332.x

Coronado, C., Candela, J., Iglesias-Prieto, R., Sheinbaum, J., López, M., & Ocampo-Torres, F. J. (2007). On the circulation in the Puerto Morelos fringing reef lagoon. *Coral Reefs*, *26*(1), 149–163. https://doi.org/10.1007/s00338-006-0175-9

Cuttler, M., Lowe, R., Hansen, J. E., Falter, J., & Pomeroy, A. (2015). Grainsize, Composition and Bedform Patterns in a Fringing Reef System. *Coastal Sediments 2015*. https://doi.org/10.1142/9789814689977_0239

Cuttler, M. V. W., Lowe, R. J., Falter, J. L., & Buscombe, D. (2017). Estimating the settling velocity of bioclastic sediment using common grain-size analysis techniques. *Sedimentology*, *64*(4), 987–1004. https://doi.org/10.1111/sed.12338

Dalrymple, R. A., MacMahan, J. H., Reniers, A. J., & Nelko, V. (2011). Rip currents. *Annual Review of Fluid Mechanics*, *43*(1), 551–581. https://doi.org/10.1146/annurev-fluid-122109-160733

de Bakker, A. T. M., Tissier, M. F. S., & Ruessink, B. G. (2014). Shoreline Dissipation of Infragravity Waves. *Continental Shelf Research*, *72*, 73–82. https://doi.org/10.1016/j.csr.2013.11.013

Emery, W. J., & Thomson, R. E. (2001). *Data analysis methods in physical oceanography*. Amsterdam, Netherlands: Elsevier Science.

Erftemeijer, P. L., Riegl, B., Hoeksema, B. W., & Todd, P. A. (2012). Environmental impacts of dredging and other sediment disturbances on corals: A review. *Marine Pollution Bulletin*, *64*(9), 1737–1765. https://doi.org/10.1016/j.marpolbul.2012.05.008

Francis, J. (1973). Experiments on the motion of solitary grains along the bed of a water-stream. *Proceedings of the Royal Society of London*, *332*, 443–471. https://doi.org/10.1098/rspa.1973.0037

Goring, D., & Nikora, V. (2002). Despiking acoustic Doppler velocimeter data. *Journal of Hydraulic Engineering*, *128*(1), 117–126. https://doi.org/10.1061/(ASCE)0733-9429(2002)128:1(117)

Gourlay, M. R. (1994). Wave transformation on a coral reef. *Coastal Engineering*, *23*(1–2), 17–42. https://doi.org/10.1016/0378-3839(94)90013-2

Gourlay, M. R. (1996a). Wave set-up on coral reefs. 1. Set-up and wave-generated flow on an idealised two dimensional horizontal reef. *Coastal Engineering*, *27*(3–4), 161–193. https://doi.org/10.1016/0378-3839(96)00008-7

Gourlay, M. R. (1996b). Wave set-up on coral reefs. 2. Set-up on reefs with various profiles. *Coastal Engineering*, *28*(1–4), 17–55. https://doi.org/10.1016/0378-3839(96)00009-9

Gourlay, M. R., & Colleter, G. (2005). Wave-generated flow on coral reefs—An analysis for two-dimensional horizontal reef-tops with steep faces. *Coastal Engineering*, *52*(4), 353–387. https://doi.org/10.1016/j.coastaleng.2004.11.007

Grant, W. D., & Madsen, O. S. (1979). Combined wave and current interaction with a rough bottom. *Journal of Geophysical Research*, *84*, 1797–1808. https://doi.org/10.1029/JC084iC04p01797

Ha, H., Maa, J.-Y., Park, K., & Kim, Y. (2011). Estimation of high-resolution sediment concentration profiles in bottom boundary layer using pulse-coherent acoustic Doppler current profilers. *Marine Geology*, *279*(1-4), 199–209. https://doi.org/10.1016/j.margeo.2010.11.002

Hardy, T. A., & Young, I. R. (1996). Field study of wave attenuation on an offshore coral reef. *Journal of Geophysical Research*, *101*, 14,311–14,326. https://doi.org/10.1029/96JC00202

Harney, J. N., & Fletcher, C. H. (2003). A budget of carbonate framework and sediment production, Kailua Bay, Oahu, Hawaii. *Journal of Sedimentary Research*, *73*(6), 856–868. https://doi.org/10.1306/051503730856

Harris, D. L., Vila-Concejo, A., & Webster, J. M. (2014). Geomorphology and sediment transport on a submerged back-reef sand apron: One tree reef, great barrier reef. *Geomorphology*, *222*, 132–142. https://doi.org/10.1016/j.geomorph.2014.03.015

Hearn, C. J. (1999). Wave-breaking hydrodynamics within coral reef systems and the effect of changing relative sea level. *Journal of Geophysical Research*, *104*, 30,007–30,019. https://doi.org/10.1029/1999JC900262

Hench, J. L., Leichter, J. J., & Monismith, S. G. (2008). Episodic circulation and exchange in a wave-driven coral reef and lagoon system. *Limnology and Oceanography*, *53*(6), 2681–2694. https://doi.org/10.4319/lo.2008.53.6.2681

Hine, A. C., Wilber, R. J., Bane, J. M., Neumann, A. C., & Lorenson, K. R. (1981). Offbank transport of carbonate sands along open, leeward bank margins: Northern Bahamas. *Sedimentary Dynamics of Continental Shelves*, *42*(1-4), 327–348. https://doi.org/10.1016/0025-3227(81)90169-9

Hoitink, A. J. F. (2004). Tidally-induced clouds of suspended sediment connected to shallow-water coral reefs. *Marine Geology*, *208*(1), 13–31. https://doi.org/10.1016/j.margeo.2004.04.021

Hubbard, D. K. (1986). Sedimentation as a control of reef development: St. Croix, U.S.V.I. *Coral Reefs*, *5*(3), 117–125. https://doi.org/10.1007/BF00298179

Hughes, T. (1999). Off-reef transport of coral fragments at Lizard Island, Australia. *Marine Geology*, *157*(1-2), 1–6. https://doi.org/10.1016/S0025-3227(98)00187-X

Jago, O., Kench, P., & Brander, R. (2007). Field observations of wave-driven water-level gradients across a coral reef flat. *Journal of Geophysical Research*, *112*, C06027. https://doi.org/10.1029/2006JC003740

Jokiel, P. L., Rodgers, K. S., Storlazzi, C. D., Field, M. E., Lager, C. V., & Lager, D. (2014). Response of reef corals on a fringing reef flat to elevated suspended-sediment concentrations: Moloka'i, Hawai'i. *Peer J*, *2*, e699. https://doi.org/10.7717/peerj.699

Kench, P. S. (1998a). A currents of removal approach for interpreting carbonate sedimentary processes. *Marine Geology*, *145*(3-4), 197–223. https://doi.org/10.1016/S0025-3227(97)00101-1

Kench, P. S. (1998b). Physical controls on development of lagoon sand deposits and lagoon infilling in an Indian Ocean atoll. *Journal of Coastal Research*, *14*, 1014–1024.

Kennedy, D. ., & Woodroffe, C. (2000). Holocene lagoonal sedimentation at the latitudinal limits of reef growth, Lord Howe Island, Tasman Sea. *Marine Geology*, *169*(3-4), 287–304. https://doi.org/10.1016/S0025-3227(00)00093-1

Larcombe, P., Costen, A., & Woolfe, K. J. (2001). The hydrodynamic and sedimentary setting of nearshore coral reefs, central Great Barrier Reef shelf, Australia: Paluma Shoals, a case study. *Sedimentology*, *48*(4), 811–835. https://doi.org/10.1046/j.1365-3091.2001.00396.x

Le Bouteiller, C., & Venditti, J. G. (2015). Sediment transport and shear stress partitioning in a vegetated flow. *Water Resources Research*, *51*, 2901–2922. https://doi.org/10.1002/2014WR015825

Longuet-Higgins, M. S., & Stewart, R. W. (1962). Radiation stress and mass transport in gravity waves, with application to 'surf beats'. *Journal of Fluid Mechanics*, *13*(04), 481–504. https://doi.org/10.1017/S0022112062000877

Longuet-Higgins, M. S., & Stewart, R. W. (1964). Radiation stresses in water waves—A physical discussion, with applications. *Deep-Sea Research*, *11*(4), 529–562. https://doi.org/10.1016/0011-7471(64)90001-4

Lowe, R. J., & Falter, J. L. (2015). Oceanic forcing of coral reefs. *Annual Review of Marine Science*, *7*(1), 43–66. https://doi.org/10.1146/annurev-marine-010814-015834

Lowe, R. J., Falter, J. L., Bandet, M. D., Pawlak, G., Atkinson, M. J., Monismith, S. G., & Koseff, J. R. (2005). Spectral wave dissipation over a barrier reef. *Journal of Geophysical Research*, *110*, C04001. https://doi.org/10.1029/2004JC002711

Lowe, R. J., Falter, J. L., Monismith, S. G., & Atkinson, M. J. (2009). A numerical study of circulation in a coastal reef-lagoon system. *Journal of Geophysical Research*, *114*, C06022. https://doi.org/10.1029/2008JC005081

Lowe, R. J., Koseff, J., & Monismith, S. G. (2005). Oscillatory flow through submerged canopies: 1. Velocity structure. *Journal of Geophysical Research*, *110*, C10016. https://doi.org/10.1029/2004JC002788

Lowe, R. J., Shavit, U., Falter, J. L., Koseff, J. R., & Monismith, S. G. (2008). Modeling flow in coral communities with and without waves: A synthesis of porous media and canopy flow approaches. *Limnology and Oceanography*, *53*(6), 2668–2680. https://doi.org/10.4319/lo.2008.53.6.2668

Lugo-Fernández, A., Roberts, H. H., Wiseman, W. J. Jr., & Carter, B. L. (1998). Water level and currents of tidal and infragravity periods at Tague Reef, St. Croix (USVI). *Coral Reefs*, *17*(4), 343–349. https://doi.org/10.1007/s003380050137

Luhar, M., Coutu, S., Infantes, E., Fox, S., & Nepf, H. (2010). Wave-induced velocities inside a model seagrass bed. *Journal of Geophysical Research*, *115*, C12005. https://doi.org/10.1029/2010JC006345

Madsen, O. S. (1994). Spectral wave-current bottom boundary layer flows. *Coastal Engineering Proceedings*, *1*(24). https://doi.org/10.1061/9780784400890.030

Madsen, O. S., Poon, Y.-K., & Graber, H. C. (1988). Spectral wave attenuation by bottom friction: Theory. *Coastal Engineering Proceedings*, *1*(21). Retrieved from https://journals.tdl.org/icce/index.php/icce/article/viewArticle/4241

Massel, S. R., & Gourlay, M. R. (2000). On the modelling of wave breaking and set-up on coral reefs. *Coastal Engineering*, *39*(1), 1–27. https://doi.org/10.1016/S0378-3839(99)00052-6

Mathisen, P. P., & Madsen, O. S. (1999). Waves and currents over a fixed rippled bed 3. Bottom and apparent roughness for spectral waves and currents. *Journal of Geophysical Research*, *104*, 18,447–18,461. https://doi.org/10.1029/1999JC900114

Monismith, S. G. (2007). Hydrodynamics of coral reefs. *Annual Review of Fluid Mechanics*, *39*(1), 37–55. https://doi.org/10.1146/annurev.fluid.38.050304.092125

Morgan, K. M., & Kench, P. S. (2014). A detrital sediment budget of a Maldivian reef platform. *Geomorphology*, *222*, 122–131. https://doi.org/10.1016/j.geomorph.2014.02.013

Nielsen, P. (1992). *Coastal bottom boundary layers and sediment transport* (Vol. 4). Singapore: World Scientific. https://doi.org/10.1142/1269

Ogston, A. S., Storlazzi, C. D., Field, M. E., & Presto, M. K. (2004). Sediment resuspension and transport patterns on a fringing reef flat, Molokai, Hawaii. *Coral Reefs*, *23*(4), 559–569. https://doi.org/10.1007/s00338-004-0415-9

O'Hara Murray, R. B., Thorne, P., & Hodgson, D. (2011). Intrawave observations of sediment entrainment processes above sand ripples under irregular waves. *Journal of Geophysical Research*, *116*, C01001. https://doi.org/10.1029/2010JC006216

Péquignet, A.-C. N., Becker, J. M., & Merrifield, M. A. (2014). Energy transfer between wind waves and low-frequency oscillations on a fringing reef, Ipan, Guam. *Journal of Geophysical Research: Oceans*, *119*, 6709–6724. https://doi.org/10.1002/2014JC010179

Péquignet, A.-C. N., Becker, J. M., Merrifield, M. A., & Aucan, J. (2009). Forcing of resonant modes on a fringing reef during tropical storm Man-Yi. *Geophysical Research Letters*, *36*, L03607. https://doi.org/10.1029/2008GL036259

Perry, C. T., & Hepburn, L. J. (2008). Syn-depositional alteration of coral reef framework through bioerosion, encrustation and cementation: Taphonomic signatures of reef accretion and reef depositional events. *Earth-Science Reviews*, *86*(1–4), 106–144. https://doi.org/10.1016/j.earscirev.2007.08.006

Perry, C. T., Kench, P. S., Smithers, S. G., Riegl, B., Yamano, H., & O'Leary, M. J. (2011). Implications of reef ecosystem change for the stability and maintenance of coral reef islands. *Global Change Biology*, *17*(12), 3679–3696. https://doi.org/10.1111/j.1365-2486.2011.02523.x

Pomeroy, A. W. M., Lowe, R. J., Ghisalberti, M., Storlazzi, C. D., Symonds, G., & Roelvink, D. (2017). Sediment transport in the presence of large reef bottom roughness. *Journal of Geophysical Research: Oceans*, *122*, 1347–1368. https://doi.org/10.1002/2016JC011755

Pomeroy, A. W. M., Lowe, R. J., Symonds, G., Van Dongeren, A., & Moore, C. (2012). The dynamics of infragravity wave transformation over a fringing reef. *Journal of Geophysical Research*, *117*, C11022. https://doi.org/10.1029/2012JC008310

Presto, M. K., Ogston, A. S., Storlazzi, C. D., & Field, M. E. (2006). Temporal and spatial variability in the flow and dispersal of suspended-sediment on a fringing reef flat, Molokai, Hawaii. *Estuarine, Coastal and Shelf Science*, *67*(1-2), 67–81. https://doi.org/10.1016/j.ecss.2005.10.015

Roeber, V., & Bricker, J. D. (2015). Destructive tsunami-like wave generated by surf beat over a coral reef during typhoon Haiyan. *Nature Communications*, *6*(1), 7854. https://doi.org/10.1038/ncomms8854

Rogers, C. S. (1990). Responses of coral reefs and reef organisms to sedimentation. *Marine Ecology Progress Series*, *62*, 185–202. https://doi.org/10.3354/meps062185

Roth, M. S. (2014). The engine of the reef: Photobiology of the coral–algal symbiosis. *Frontiers in Microbiology*, *5*, 422. https://doi.org/10.3389/fmicb.2014.00422

Roy, K. J., & Smith, S. V. (1971). Sedimentation and coral reef development in turbid water: Fanning Lagoon. *Pacific Science*, *25*(2), 234–248. http://hdl.handle.net/10125/4240

Sanderson, P. G., & Eliot, I. (1996). Shoreline salients, cuspate forelands and tombolos on the coast of Western Australia. *Journal of Coastal Research*, *12*(3), 761–773.

Schmidt, W. E., Guza, R. T., & Slinn, D. N. (2005). Surf zone currents over irregular bathymetry: Drifter observations and numerical simulations. *Journal of Geophysical Research*, *110*, C12015. https://doi.org/10.1029/2004JC002421

Schoellhamer, D. H. (2002). Variability of suspended-sediment concentration at tidal to annual time scales in San Francisco Bay, USA. *Continental Shelf Research*, *22*(11–13), 1857–1866. https://doi.org/10.1016/S0278-4343(02)00042-0

Scoffin, T. P. (1992). Taphonomy of coral reefs: A review. *Coral Reefs*, *11*(2), 57–77. https://doi.org/10.1007/bf00357423

Sheremet, A., Kaihatu, J. M., Su, S. F., Smith, E. R., & Smith, J. M. (2011). Modeling of nonlinear wave propagation over fringing reefs. *Coastal Engineering*, *58*(12), 1125–1137. https://doi.org/10.1016/j.coastaleng.2011.06.007

Shields, A. (1936). Application of similarity principles and turbulence research to bed-load movement.

Soulsby, R., & Clarke, S. (2005). Bed shear-stresses under combined waves and currents on smooth and rough beds. *HR Wallingford, Report TR137*.

Stearn, C. W., Scoffin, T. P., & Martindale, W. (1977). Calcium carbonate budget of a fringing reef on the west coast of Barbados. Part I—Zonation and productivity. *Bulletin of Marine Science*, *27*(3), 479–510.

Stocking, J. B., Rippe, J. P., & Reidenbach, M. A. (2016). Structure and dynamics of turbulent boundary layer flow over healthy and algae-covered corals. *Coral Reefs*, *35*(3), 1047–1059. https://doi.org/10.1007/s00338-016-1446-8

Storlazzi, C. D., Field, M. E., Bothner, M. H., Presto, M. K., & Draut, A. E. (2009). Sedimentation processes in a coral reef embayment: Hanalei Bay, Kauai. *Marine Geology*, *264*(3-4), 140–151. https://doi.org/10.1016/j.margeo.2009.05.002

Storlazzi, C. D., Norris, B. K., & Rosenberger, K. J. (2015). The influence of grain size, grain color, and suspended-sediment concentration on light attenuation: Why fine-grained terrestrial sediment is bad for coral reef ecosystems. *Coral Reefs*, 1–9.

Storlazzi, C. D., Ogston, A. S., Bothner, M. H., Field, M. E., & Presto, M. K. (2004). Wave- and tidally-driven flow and sediment flux across a fringing coral reef: Southern Molokai, Hawaii. *Continental Shelf Research*, *24*(12), 1397–1419. https://doi.org/10.1016/j.csr.2004.02.010

Suhayda, J. N., & Roberts, H. H. (1977). Wave action and sediment transport on frinigng reefs. In D. L. Taylor (Ed.), *Proceedings of Third International Coral Reef Symposium Vol. 2: Geology. Rosenstiel School of Marine and Atmospheric Science* (pp. 65–70). Miami, FL.

Symonds, G., Black, K. P., & Young, I. R. (1995). Wave-driven flow over shallow reefs. *Journal of Geophysical Research*, *100*, 2639–2648. https://doi.org/10.1029/94JC02736

Symonds, G., Huntley, D. A., & Bowen, A. J. (1982). Two dimensional surfbeat: Long wave generation by a time varying breakpoint. *Journal of Geophysical Research*, *87*, 492–498. https://doi.org/10.1029/JC087iC01p00492

Taebi, S., Lowe, R. J., Pattiaratchi, C. B., Ivey, G. N., & Symonds, G. (2012). A numerical study of the dynamics of the wave-driven circulation within a fringing reef system. *Ocean Dynamics*, *62*(4), 585–602. https://doi.org/10.1007/s10236-011-0514-4

Taebi, S., Lowe, R. J., Pattiaratchi, C. B., Ivey, G. N., Symonds, G., & Brinkman, R. (2011). Nearshore circulation in a tropical fringing reef system. *Journal of Geophysical Research*, *116*, C02016. https://doi.org/10.1029/2010JC006439

Thorne, P. D., Davies, A. G., & Williams, J. J. (2003). Measurements of near-bed intra-wave sediment entrainment above vortex ripples. *Geophysical Research Letters*, *30*(20), 2028. https://doi.org/10.1029/2003GL018427

Traykovski, P., Hay, A. E., Irish, J. D., & Lynch, J. F. (1999). Geometry, migration, and evolution of wave orbital ripples at LEO-15. *Journal of Geophysical Research*, *104*, 1505–1524. https://doi.org/10.1029/1998JC900026

Tudhope, A. W., & Scoffin, T. P. (1994). Growth and structure of fringing reefs in a muddy environment, South Thailand. *Journal of Sedimentary Research*, *64*(4).

Van Rijn, L. C. (1984a). Sediment transport, part I: Bed load transport. *Journal of Hydraulic Engineering*, *110*(10), 1431–1456. https://doi.org/10.1061/(ASCE)0733-9429(1984)110:10(1431)

Van Rijn, L. C. (1984b). Sediment transport, part II: Suspended load transport. *Journal of Hydraulic Engineering*, *110*(11), 1613–1641. https://doi.org/10.1061/(ASCE)0733-9429(1984)110:11(1613)

Van Rijn, L. C. (2007). Unified view of sediment transport by currents and waves. III: Graded beds. *Journal of Hydraulic Engineering*, *133*(7), 761–775. https://doi.org/10.1061/(ASCE)0733-9429(2007)133:7(761)

van Thiel de Vries, J. S. M., van Gent, M. R. A., Walstra, D. J. R., & Reniers, A. J. H. M. (2008). Analysis of dune erosion processes in large-scale flume experiments. *Coastal Engineering*, *55*, 1028–1040.

Vautard, R., Yiou, P., & Ghil, M. (1992). Singular-spectrum analysis: A toolkit for short, noisy chaotic signals. *Physica D: Nonlinear Phenomena*, *58*(1–4), 95–126. https://doi.org/10.1016/0167-2789(92)90103-T

Vila-Concejo, A., Harris, D. L., Power, H. E., Shannon, A. M., & Webster, J. M. (2014). Sediment transport and mixing depth on a coral reef sand apron. *Geomorphology*, *222*, 143–150. https://doi.org/10.1016/j.geomorph.2013.09.034

Weber, M., de Beer, D., Lott, C., Polerecky, L., Kohls, K., Abed, R. M., et al. (2012). Mechanisms of damage to corals exposed to sedimentation. *Proceedings of the National Academy of Sciences*, *109*(24), E1,558–E1,567. https://doi.org/10.1073/pnas.1100715109

Woodroffe, C., McLean, R., Smithers, S., & Lawson, E. (1999). Atoll reef-island formation and response to sea-level change: West Island, Cocos (Keeling) Islands. *Marine Geology*, *160*(1–2), 85–104. https://doi.org/10.1016/S0025-3227(99)00009-2